

**IN THE UNITED STATES PATENT AND TRADEMARK OFFICE**

Applicant(S) : Davids, et al  
Serial No. : 10/706,691  
For : CYTOKINE ANTAGONIST MOLECULE  
Filed : November 12, 2003  
Examiner : Shulamith H. Shafer  
Art Unit : 1647  
Confirmation No. : 5783

745 Fifth Avenue  
New York, NY 10151

**FILED VIA EFS-WEB  
ON APRIL 23, 2009**

**DECLARATION OF DR. URSULA BOSCHERT UNDER 37 C.F.R. § 1.132**

Commissioner for Patents  
P.O. Box 1450  
Alexandria, VA 22313-1450

Dear Sir:

I, Dr. Ursula Boschert, declare and state:

1. A copy of my *curriculum vitae* demonstrating my education, training and experience is attached. I am familiar with U.S. application Serial No. 10/706,691 and its prosecution history. I am considered by my peers to be an expert in the field to which the application pertains, and am otherwise qualified to speak and render expert opinions as to the present application, invention, and issues of the Office Action dated December 23, 2008. Thus, this Declaration is in response to the Office Action.

2. The following experiments were performed under my direction, supervision or control, and in the ordinary course of business.

## **Example 1: Cytokine expression modulation properties of INSP052EC-6His in LPS-induced cytokine release in mice**

### 1.1: Introduction

The ability of INSP052EC to protect from the effects of cytokine release in vivo has been also tested by injecting either the recombinant protein or encapsulated, transiently transfected HEK293 cells expressing INSP052EC-6His in the model of LPS-induced TNF alpha and IL-6 release in mice.

Encapsulation of cells expressing a recombinant protein allows understanding of the possible therapeutic effects of a continuous administration of the protein in vivo, as shown with proteins with tumor suppressor function, for example (Visted T *et al.*, 2003, *Hum Gene Ther.*, 14, 1429-40).

LPS (Lipopolysaccharides) are an important component of the outer membranes of gramnegative bacteria and are the best characterised example of innate recognition that leads to a robust inflammatory response by macrophages or microglia cells via its binding to CD14 and the Toll receptor 4 (Lehnardt S *et al.*, 2002, *J Neurosci.*, 22, 2478-2486). LPS are widely used in literature to activate various cell types like macrophages, microglia and endothelial cells, in particular in relationship to liver diseases (Jirillo E *et al.*, 2002, *J Endotoxin Res.*, 8, 319-327).

### 1.2: Materials & Methods

#### 1.2.1: Encapsulation of transiently transfected HEK293 cells expressing INSP052EC6His

##### 1.2.1.1: Cell maintenance

Human Embryonic Kidney 293 cells expressing the Epstein-Barr virus Nuclear Antigen (HEK293-EBNA, Invitrogen) were maintained in suspension in Ex-cell VPRO serum-free medium (maintenance medium, JRH, UK) supplemented with 4mM L-Glutamine (Invitrogen) and 1ml/L Phenol-Red-solution (0.5% w/v in water, Phenol Red: Sigma, USA) in spinner flasks (Techne, UK).

##### 1.2.1.2: Cell transfection

At the day of transfection cells were centrifuged and re-suspended in a spinner vessel (DasGip, D) in 250 mL DMEM / F12 (1:1) medium containing 1% FBS and 4ml/1 ITS-X

supplement (seeding medium, all Invitrogen) at a density of  $1 \times 10^6$  cells/ml. Cells were transfected using the PEI method with a ratio of 2: 1 PEI:DNA. In 100 mL seeding medium 50011 g of corresponding plasmid (pDESTI2.2-INSP052EC) was mixed with 1 mg PEI (Polysciences, USA) and incubated for 10 minutes at room temperature. The mixture was added to the cell suspension and incubated for 90 minutes at 37°C. After the incubation the cell suspension was centrifuged (200xg, 10 minutes at 4°C) and the cell pellet was re-suspended in 500 ml maintenance medium. Cells were incubated in a humidified atmosphere with 5% CO<sub>2</sub> at 37°C until encapsulation.

#### 1.2.1.3: Cell encapsulation

HEK293EBNA cells transfected with pDESTI2.2-INSP052EC or not transfected (control cells) were encapsulated into Alginate-poly-L-Lysine-Alginate (APA) capsules using the Inotech research encapsulator (Inotech, CH). Cells were centrifuged (200xg 10min 4°C) and re-suspended in 2 ml washing buffer (all chemicals Inotech, CH). To this suspension a 1.5% alginate solution was slowly added to yield a final cell concentration of  $2.5 \times 10^6$  cells/ml solution. The alginate-cell-suspension was taken up into a syringe (Braun Omnifit, Braun, D), which was connected to the encapsulation machine.

The encapsulation was carried out using the following parameters:

- Syringe Pump: 275 (50ml Syringe) or 456 (20ml Syringe)
- Anode voltage: 1.16kV
- Vibration frequency: 1943 Hz
- Vibration amplitude: 3

The protocol for encapsulation was the following:

- Polymerisation buffer: 10 minutes (volume 250 ml)
- Poly-L-Lysin: 10 minutes (volume 150 ml)
- Washing buffer: 1 minute (volume 150 ml)
- Washing buffer: 5 minutes (volume 150 ml)
- 0.03% Alginate: 5 minutes (volume 150 ml)
- Washing buffer: 1 minute (volume 150 ml)
- Depolymerisation buffer: 10 minutes (volume 300 ml)
- Washing buffer: 1 minute (volume 150 ml)

- Washing buffer: 5 minutes (volume 150 ml)
- Medium (Excell-V-Pro): volume 100 ml

All buffers were prepared according to the manufacturer's manual in sterile distilled water under sterile conditions. In the final step of the encapsulation, the capsules were resuspended in 100 ml maintenance medium and transferred into a sterile spinner vessel (Dasgip, D). The capsules were incubated in a humidified atmosphere with 5% CO<sub>2</sub> at 37°C overnight or until injection into the animals.

#### 1.2.2: LPS induced cytokine release model in vivo

The model of LPS-induced TNF alpha and IL-6 release in mice was set up according to W098/38179. Briefly, male C57/BL6 or C3H/HeN mice (8 weeks of age; Charles River, France) were used. In general, 10 animals per experimental group are used. Mice were maintained in standard conditions under a 12-hour light-dark cycle, provided irradiated food and water ad libitum.

LPS (0111:B4 (Sigma, Switzerland), 0.3 mg/kg) was injected s.c in mice. Ninety minutes later blood was sampled and plasma TNF alpha was determined using an ELISA kit (R&D). IL-6 levels were measured after 150 minutes using a commercial available ELISA kit (R&D DuoSet ref. DY206). Dexamethasone, the reference compound, was solubilized in PBS and Dexamethasone (0.1 mg/kg, s.c.) was injected 15 minutes prior LPS.

The suspension containing the microcapsules containing HEK293 cells (control cells or cells transiently expressing INSP052EC-6His) was removed from the incubator and left several minutes in the laminar flow hood to allow the capsules to sediment. The clear supernatant was removed and the concentrated capsules were taken up carefully into a syringe. 700µl capsules were injected slowly i.p. via a 0.7 mm needle (ref 53158.01 Polylabo, CH) per mouse. LPS injection was performed at day 3 after the injection of the capsules.

#### 1.3: Results

The potential of INSP052EC to downregulate LPS-induced TNF alpha or IL-6 release in the blood was demonstrated in both models of INSP052EC administration.

The injection of INSP052EC-6His 15 minutes prior to the LPS injection. decreases LPS induced release of IL-6 (if INSP052EC-6His is administered at least at 0.1 mg/kg) and TNF alpha (if INSP052EC-6His is administered at least at 1 mg/kg) in a statistically significant manner, similarly to the reference compound Dexamethasone. Mice injected with the vehicle solution for injection (PBS-BSA with 0.02% glycerol) were used as negative controls (Figure 1).

Similar positive effects were observed when the HEK293 cells transiently expressing INSP052EC-6His were injected in all the tested capsule volumes (Figure 2).

## **Example 2: Properties of INSP052EC-6His in a model of Contact Hypersensitivity**

### 2.1: Introduction

INSP052EC was tested on hapten induced contact hypersensitivity (CHS), a murine model of inflammatory skin disease. CHS is a T cell-mediated inflammation model of the skin that represents a well established model for similar inflammations associated to diseases such allergic contact dermatitis and psoriasis, which are dermatological problems with unmet medical needs related to excessive cytokine production (Nakae S et al., 2003, Int Immunol., 15: 251-260; Gorbachev AV and Fairchild RL, 2001, Crit Rev Immunol., 21: 451-72).

### 2.2: Material and Methods

The hapten DNFB (2,4-dinitrofluorobenzene; Sigma Chemical Co.) was diluted in acetone / olive oil (4:1) immediately before use. Mice were sensitized with 30  $\mu$ l of 0.5% DNFB solution painted to the shaved dorsal skin or left untreated. Mice were challenged five days later, *i.e.* CHS was elicited by applying a non-irritant dose of 10  $\mu$ l of 0.2% DNFB onto both sides of the right ear and the same amount of solvent alone onto the left ear. Ear thickness was monitored at day 6 using a caliper (Mitutoya).

Ear swelling was calculated as

$$((T_6 - T_5) \text{ right ear}) - ((T_6 - T_5) \text{ left ear})$$

where  $T_6$  and  $T_5$  represent values of ear thickness at day 6 and day 5, respectively, after sensitization challenge, respectively. To assure that the observed swelling was due to DNFB specific inflammation rather than non-specific irritation, a non-sensitized but

challenged group of mice was included with each experiment.

Mice were treated on Day 5 with an s.c injection of INSP052EC-6His in the indicated amount, Dexamethasone (1 mg/kg), or PBS only (control group).

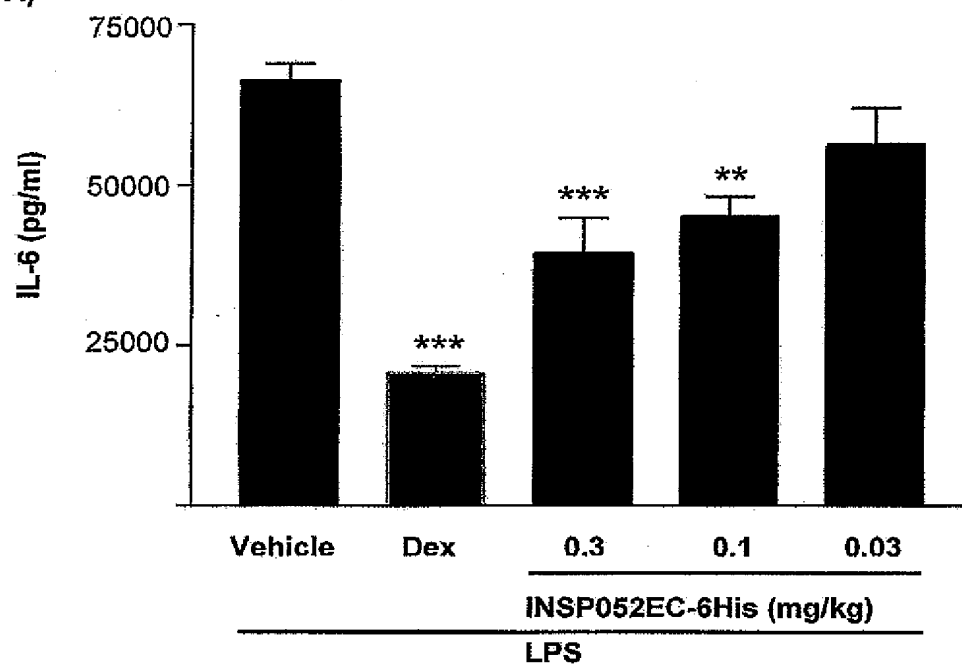
### 2.3: Results

We show that INSP052EC reduces ear swelling in significant and dose dependent manner, suggesting a decrease in leukocyte infiltration and of the consequent inflammation (Figure 3), demonstrating that INSP052EC can be useful in treating T cell-mediated inflammation of the skin, such as allergic contact dermatitis and psoriasis.

The examples clearly show that the isolated extracellular domain of INSP052 (INSP052EC) can be used (as such or as a variant or a fusion protein containing this protein sequence or the full length protein) for modulating cytokine activities, in particular as antagonist of cytokine secretion and/or expression, and may have a therapeutic role in diseases directly or indirectly related to both innate and adaptive immune responses.

The range of inhibiting activities shown by the tested INSP052EC-based molecule in different cell-based assays and animal models confirms that patho-physiological effects of cytokines resulting from their excessive or inappropriately localized production can be blocked by using this molecule. The control of cellular events associated to prolonged production of proinflammatory cytokines can be obtained by INSP052EC-based molecules, which therefore can be used for antagonizing abnormal inflammatory states associated, in particular, to autoimmune and inflammatory diseases affecting various tissues and organs (e.g. liver, skin, lungs, central nervous system), providing as well a new therapeutic opportunity for oncological, neurological, cardiovascular, and infectious disorders. Additional clinical applications for INSP052EC-based molecules can be identified by using cytokine assays showing the excessive expression and / or secretion of cytokines in samples obtained by patients affected by other diseases (Wong CK and Lam CW, Adv Clin Chem. 2003, 37:1-46; Whiteside TL, Biotechniques, 2002, Oct. Suppl:4-8, 10, 12-5), then justifying the therapeutic use of a cytokine antagonist as INSP052ECbased molecules.

**Figure 1**  
**A)**



**B)**

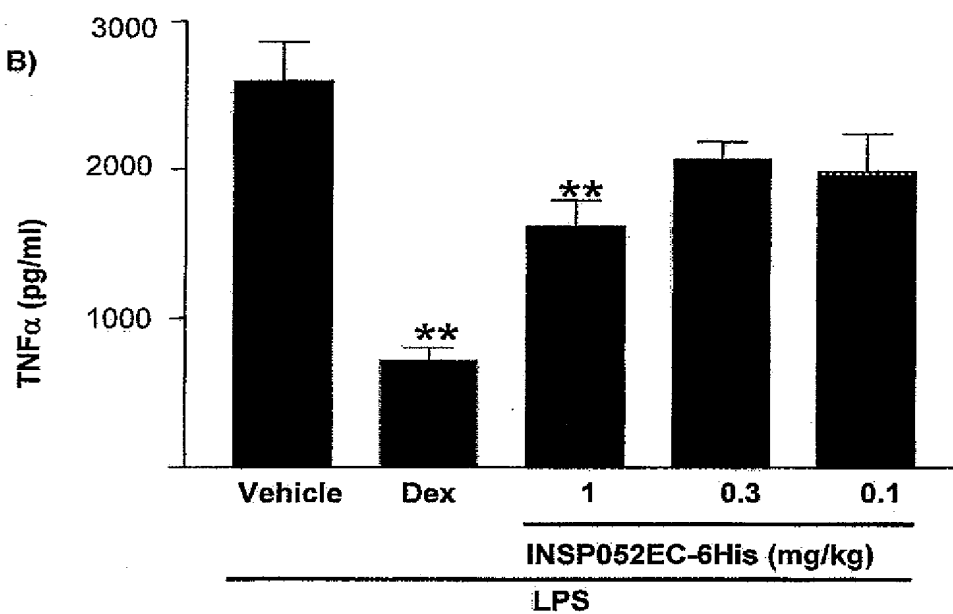


**Figure 2**

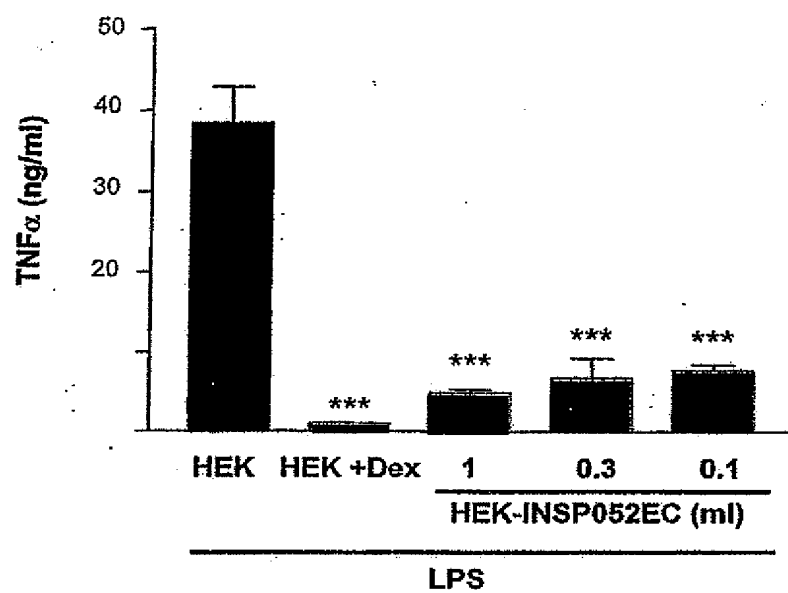
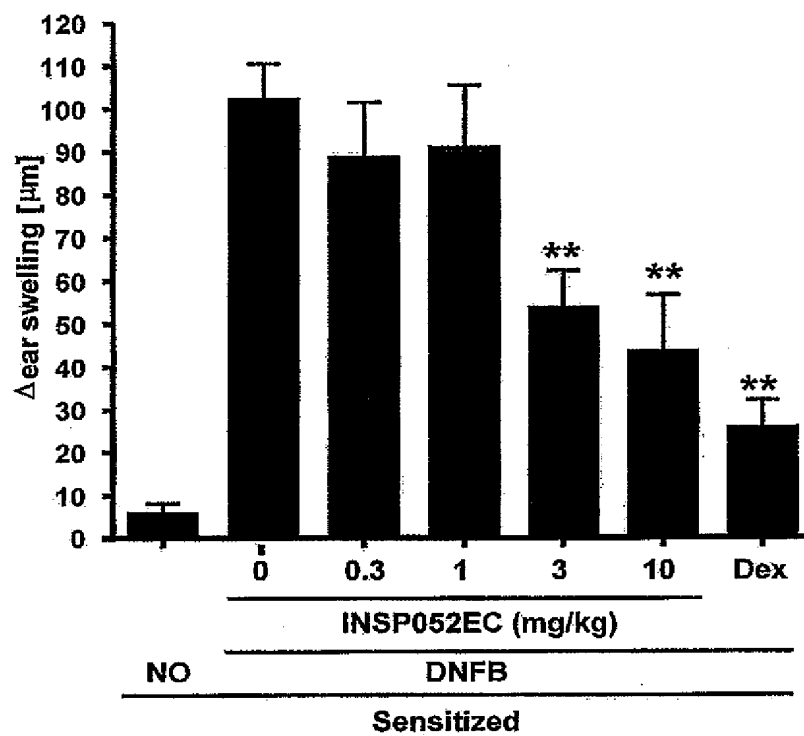




Figure 3



3. It is respectfully submitted that the data contained herein directly refutes the enablement rejection of claims under 35 U.S.C. §112, first paragraph, in the Office Action. Reconsideration and withdrawal of the rejection are solicited.

4. I further declare that all statements made herein of my own knowledge are true and that all statements made on information and belief are believed to be true and further, that the statements were made with the knowledge that willful false statements and the like so made are punishable by fine or imprisonment, or both, under Section 1001 of Title 18 of the United States Code and that such willful false statements may jeopardize the validity of the application or any patent issued thereon.

Date: 23.4.2009

Ursula Boschert  
Dr. Ursula Boschert

# Ursula Boschert, PhD

## Business Address

MerckSerono Geneva Research Institute (GRC)  
Therapeutic Area Neurodegeneration (TA NDD)  
e-mail: [ursula.boschert@merckserono.net](mailto:ursula.boschert@merckserono.net)  
Office: 0224149731, Mobile : 0795988773

## Date of birth/personal data

31.03.1959 in Oberkirch/Germany, married, 1 child

## Career Objective:

**To build and maintain world-class functional excellence in Neuroimmunology**

## Profile

- 15 years of experience in target validation and drug discovery with strong expertise in *in vitro* and *in vivo* pharmacology of NDD diseases (Multiple Sclerosis, Peripheral Neuropathy, Alzheimer Disease, Psychiatric Disorders)
- Formulated new concepts for discovery of new targets in Neuroimmunology
- Project leader and team member of discovery projects involved in the identification, characterization and development of biologicals and small molecules supporting projects up to Phase I
- Participation in cross-TA evaluation of MerckSerono discovery projects (go, no/go recommendations)
- Experience in target classes including GPCRs (serotonin -, chemokine -, S1P- receptor subtypes), cytokines (osteopontin, TNF $\alpha$ ), metalloproteases (MMP-2, MMP-9, MMP-12), adhesion molecules (immunoglobulin superfamily, integrins –  $\alpha\beta3$ ,  $\alpha\beta5$ ,  $\alpha4\beta1$ ), MAP kinase phosphatases (Pac1, MKP3, MKP4)
- Driver of academic and clinical research collaborations in support of novel technologies, targets and assays for NBEs or NCEs
- Organisation of an advisory board meeting involving clinical and academic experts in the field of Diabetic Neuropathy
- Support of Business Development in the Evaluation /Due Diligences of early and late phase opportunities
- Responsible for up to 9 direct reports in the past
- Current Group: 2 scientists, 1 technical expert, 2 assistant scientists and ongoing recruitment of 3 technicians
- Supervision of 4 Diploma students, 3 PhD students, 2 postdocs and member of the student committee
- Good communication skills involving interaction with other functions of research and development
- Result oriented, innovative, enthusiastic and able to quickly adapt to new developments and tasks

## Professional Experience

2008	<b>Senior Research Scientist/Group Leader</b> Neuroimmunology Therapeutic Area NDD (Dr. E. Sedman) MerckSerono Research Center, Geneva
2004 - 2007	<b>Senior Research Scientist/Group Leader</b> Immunology Department (Dr. Y. Chvatchko) Serono Pharmaceutical Research Institut, Geneva
2001-2004	<b>Senior Research Scientist</b> Immunology Department (Dr. M. Kosco, Dr. Y. Chvatchko) Serono Pharmaceutical Research Institut, Geneva
1998- 2001	<b>Research Scientist II</b> Neurobiology Department (Dr. S. Arkinstall, Dr. R. Papoian) Serono Pharmaceutical Research Institute, Geneva
1994 -1997	<b>Research Scientist I</b> Neurobiology Department (Dr. S.Catsicas) Glaxo Wellcome, Geneva
1990 - 1993	<b>Postdoctoral fellow</b> (Dr. R. Hen, Prof. P. Chambon) INSERM/CNRS Strasbourg, LGME, France,
1988	<b>Visiting Fellow</b> (Prof. G. Miklos) Research School of Biological Sciences, Canberra, Australia
1986 - 1990	<b>PhD student</b> (Prof. K. Fischbach, Prof. Heisenberg) Albert-Ludwigs-Universitat Freiburg i. Brg., Germany

## AWARDS

- 2001: WO2002092122 Serono Patent Award (selected from 14 patents)
- 2005: WO2006016238 Serono Patent Award (selected from 45 patents)

## PATENTS

1. **WO2006016238** Capsules containing transfected cells, method for preparing the same and uses thereof for immunization and vaccination.
2. **WO2006095164** Lipocalin protein
3. **WO2005046714** Cytokine antagonist molecules
4. **WO2004056983** Metalloprotease proteins
5. **WO2004084932** Use of Clusterin for the treatment and/or prevention of peripheral neurological diseases
6. **WO2004113379** Interferon gamma-like protein
7. **WO2002092122** Use of osteopontin for the treatment and/or prevention of neurological diseases
8. **WO2000078331** IL6RIL6 Chimera for the treatment of neurodegenerative diseases
9. **WO1994018319** Novel polypeptides having serotonergic receptor activity (5HT1B), nucleic acids coding therefore and use of therefore
10. **WO1994001556** Novel polypeptides having serotonergic receptor activity (5HT1A), nucleic acids coding therefore and use of therefore
11. **WO1994001555** Novel polypeptides having serotonergic receptor activity (5HT5A, 5HT6), nucleic acids coding therefore and use of therefore

## PUBLICATIONS

1. A. Rolland, L. Favre-Kontula, L. Bernasconi, M. Karmirantzou, C. Power, B. Antonsson, **U. Boschert** (2008) GlialCAM, an immunoglobulin-like cell adhesion molecule is expressed in glial cells of the central nervous system. *Glia* 56, 633-645.
2. L. Favre-Kontula, P. Sattonnet-Roche, E. Magnenat, A.E.Proudfoot, **U. Boschert**, I Xenarios, F. Vilbois, B. Antonsson (2008) detection and identification of plasma proteins that bind GlialCAM using Protein Chip arrays, SELDI-TOF MS and nano-LC MS/MS. *Proteomics* 8, 378-88.
3. S. Carboni, **U. Boschert**, P. Gaillard, J.P. Gotteland, J.Y. Gillon, P.A. Vitte (2008) AS601245, a JNK inhibitor, reduces axon/dendrite damage and cognitive deficits after global cerebral ischaemia in gerbils. *Br J Pharmacology* 153, 157-63.
4. L. Kadi, R. Selvaraju, P. de Lys, A.E. Proudfoot, T. N. Wells, **U. Boschert** (2006) Differential effects of chemokines on oligodendrocyte precursor proliferation and myelin formation *in vitro*. *J Neuroimmunology* 174, 133-146.

5. B. Abel, S. Freigang, M.F. Bachmann, **U. Boschert**, M. Kopf (2005) Osteopontin is not required for the development of TH1 responses and viral immunity. *J Immunology* 175, 6006- 6013.
6. M.P. Mycko, R. Papoian, **U. Boschert**, C.S. Raine, K. W. Selmaj (2004) Microarray gene expression profiling of chronic active and inactive lesions in multiple sclerosis. *Clin Neurol Neurosurg* 106, 223-229.
7. R. Selvaraju, L. Bernasconi, C. Losberger, P. Graber, L. Kadi, V. Avallana-Adalid, N. Picard-Riera, A. Van Evercooren, R. Cirillo, M.Kosco-Vibois, G. Feger, R. Papoian, **U. Boschert** (2004) Osteopontin is upregulated during *in vivo* demyelination and remyelination and enhances myelin formation *in vitro*. *Mol Cell Neuroscience* 25, 707-721.
8. M.P. Mycko, R. Papoian, **U. Boschert**, C.S. Raine, K. W. Selmaj (2004) c DNA microarray analysis in multiple sclerosis lesions: detection of genes associated with diseases activity. *Brain* 126, 1048-1057.
9. **U. Boschert**, E. Merlo-Pich, G. Higgins, Allan Roses, S. Catsicas (1999) Apolipoprotein E expression by neurons surviving excitotoxic stress. *Neurobiology of Disease* 6, 508-514.
10. **U. Boschert**, R. Dickinson, M. Muda, M. Camps, S. Arkininstall (1998) Regulated expression of dual specificity phosphatases in rat brain. *Neuroreport* 9, 4081-4086.
11. M. Camps, A. Nichols, C. Gillieron, B. Antonsson, M. Muda, C. Chabert, **U. Boschert**, S. Arkininstall (1998) ERK2 MAP kinase triggers catalytic activation of dual specificity phosphatase MKP-3. *Science* 280, 1262-1265.
12. M. Camps, M. Muda, C. Chabert, **U. Boschert**, S. Arkininstall (1998) Specific induction of the dual specificity phosphatase MKP-3 in differentiating PC12 cells is associated with blockade of ERK family mitogen-activated protein kinases. *FEBS letters* 425, 271-276.
13. M. Muda, A. Theodosius, C. Gillieron, A. Smith, C. Chabert, M. Camps, **U. Boschert**, K. Davies, A. Ashworth, S. Arkininstall (1998) The N-terminal non- catalytic region of mitogen activated protein kinase phosphatase-3 (MKP3) is responsible for tight substrate binding and enzymatic specificity. *J. Biol. Chem.* 273, 9323-9329.
14. K. Maundrell, B. Antonsson, E. Magneat, M. Camps, M. Muda, C. Chabert, C. Gillieron, **U. Boschert**, E. Vial-Knecht, J.C. Martinou and S. Arkininstall (1997) Bcl-2 undergoes phosphorylation by c-Jun N-terminal kinase / Stress-activated Protein Kinases in the presence of the constitutively active GTP-binding Protein Rac1. *J. Biol. Chem.* 272, 25238 - 25243.
15. **U. Boschert**, M. Muda, M. Camps, R. Dickenson, S. Arkininstall (1997) Induction of Dual Specificity Phosphatase Pac1 in Rat Brain following Seizure Activity. *Neuroreport* 8, 3077-3080.
16. M. Muda, **U. Boschert**, B. Antonsson, C. Gillieron, C. Chabert, M. Camps, I. Martinou, S. Arkininstall (1997) Molecular cloning and functional characterization of a novel Mitogen-activated Protein Kinase Phosphatase; MKP4. *J. Biol. Chem.* 272, 5141 - 5151.
17. R. Grailhe, **U. Boschert**, R. Hen (1997) The 5-HT<sub>5</sub>, 5HT-6 and 5-HT-7 Receptors. In: *Serotonin Receptors and their ligands*. Editors: B. Olivier, I. van Wijngaarden, W. Soudijn. Elsevier Press, 311-327.
18. M. Muda, A. Theodosious, N. Rodrigues, **U. Boschert**, M. Camps, C. Gillieron, K. Davies, A. Ashworth, S. Arkininstall (1996) The dual specificity phosphatases M3/6 and MKP-3 are highly selective for inactivation of distinct mitogen-activated protein kinases. *J. Biol. Chem.* 271, 27205-27208.

19. M. Muda, **U. Boschert**, R. Dickinson, J.-C. Martinou, I. Martinou, M. Camps, W. Schlegel, S. Arkinstall (1996) MKP-3, a novel cytosolic protein -tyrosine phosphatase that exemplifies a new class of mitogen-activated protein kinase phosphatase. *J. Biol. Chem.* 271, 4319-4326.
20. **U. Boschert**, C. O'Shaughnessy, R. Dickinson, M. Tessari, C. Bendotti, S. Catsicas, E. Merlo Pich (1996) Developmental and plasticity-related differential expression of two SNAP-25 isoforms in the rat brain. *J. Comp. Neurol.* 367, 177-193.
21. **U. Boschert**, D.A. Amara, L. Segu, R. Hen (1994) The mouse 5-hydroxytryptamine<sub>1B</sub> receptor is localized predominantly on axon terminals. *Neuroscience* 58, 167 - 182.
22. H. Matthes, **U. Boschert**, N. Amlaiky, R. Grailhe, F. Muscatelli, M.G. Mattei, R. Hen (1993) The mouse 5HT<sub>5A</sub> and 5HT<sub>5B</sub> receptors define a new family of serotonin receptors: cloning, functional expression and chromosomal localization. *Mol. Pharmacol.* 43, 313-319.
23. F. Duclos, **U. Boschert**, G. Sirugo, J.L. Mandel, R. Hen, M. Koenig (1993) New gene in the region of Friedreich ataxia locus encodes a putative transmembrane protein expressed in the nervous system. *Proc. Natl. Acad. Sci. . USA* 90, 109-113.
24. F. Saudou, L. Maroteaux, N. Amlaiky, **U. Boschert**, J.L. Plassat, R. Hen (1993) The mouse 5HT<sub>1B</sub> serotonin receptor: cloning, functional expression and localization in motor control centers. In: *Serotonin and the cerebellum*. Editors: P. Trouillas and K. Fuxe, Raven Press, New York, 201-211.
25. N. Amlaiky, S. Ramboz, **U. Boschert**, J.L. Plassat, R. Hen (1992) Isolation of a mouse "5HT<sub>1E</sub>-like" serotonin receptor expressed predominantly in the hippocampus. *J. Biol. Chem.* 267, 19761-19764.
26. L. Maroteaux, F. Sadou, N. Amlaiky, **U. Boschert**, J.L. Plassat R. Hen (1992) The mouse 5HT<sub>1B</sub> receptor: cloning , functional expression and localization in motor control centers. *Proc. Natl. Acad. Sci. . USA* 89, 3020-3024.
27. J.L. Plassat, **U. Boschert**, N. Amlaiky, R. Hen (1992) The mouse 5HT<sub>5</sub> receptor reveals a considerable heterogeneity within the 5HT<sub>1D</sub> receptor family. *EMBO J.* 11, 4779-4786.
28. F. Saudou, **U. Boschert**, N. Amlaiky , J.L. Plassat, R. Hen (1992) A family of *Drosophila* serotonin receptors with distinct signalling properties and expression patterns. *EMBO J.* 11, 7-17.
29. **U. Boschert**, R.G.P. Ramos, S. Tix, G.M. Technau, K.-F. Fischbach (1990) Genetic and developmental analysis of *irreC* , a genetic function required for optic chiasm formation in *Drosophila* . *J. Neurogenetics* 6, 153-171.
30. K.F. Fischbach, F. Barleben, **U. Boschert**, A.P.M. Dittrich, B. Gschwander, B. Hoube, R. Jaeger, E. Kaltenbach, R.G.P. Ramos, G. Schlosser (1989) Developmental studies on the optic lobe of *Drosophila melanogaster* using structural brain mutants. In: *Neurobiology of sensory systems*. Editors: R.N. Singh and N. Strausfeld, 171-194.

## PUBLICATIONS IN PREPARATION

1. A new approach for FAST TRACK *in-vivo* protein evaluation: Transplantation of transiently transfected and encapsulated HEK293EBNA cells . H. Heine, P. de Lys, T. Battle and U. Boschert
2. A novel method for muscle cDNA electrotransfer – increased blood expression of hSEAP by combining hyaluronidase muscle pre-treatment and poly-L glutamate formulation of pCMV-SEAP reporter cDNA. P. Sattonnet-Roche, P. de Lys, C. Power and U. Boschert

3. SDF-1alpha processing in blood: and *in vitro* and *in vivo* cleavage study using the SELDI technology. B. Antonsson, P.de Lys, V. Dechavanne, L. Chevalier and U. Boschert.
4. Identification of novel EPOsv activities using muscle electrotransfer and protein injection in the sciatic nerve crush model. P.A. Vitte, P. Sattonnet-Roche, A. Hiver, C. Power, K Maundrel, Y. Chvatchko and U. Boschert
5. Functional activity of recombinant SDF-1 $\alpha$  and OPN-A in models of Peripheral Neuropathy. Authors TBD

## SELECTED ORAL PRESENTATIONS

- 2008 Geneva Neurology Research Symposium at Merck Serono: *"The BBB and drug discovery"*
- 2005 14<sup>th</sup> Immunology day meeting Geneva (P .de Lys, U. Boschert)  
*"FAST TRACK- identification of novel gene activities in vivo"*
- 2005 Myelin Conference, Italy: Myelin structure and its role in autoimmunity:  
*"The cytokine osteopontin promotes myelination and functional recovery in models of PN"*
- 2004 4th European Workshop on Stem Cells In Myelin Repair , Cambridge (Y. Dean, U. Boschert)  
*"Stem cell transplantation for myelin repair – cell based therapy in the MOG EAE"*
- 2003 European Brain Research Meeting, Les ARC  
*"Osteopontin – a cytokine involved in inflammation and NS repair"*
- 2002 12<sup>th</sup> Immunology Day meeting, Geneva (R. Selvaraju, U. Boschert):  
*"The TH1-cytokine osteopontin (ETA-1) plays a role in the regulation of central nervous system myelination"*
- 1997 International Meeting on Alzheimer Disease, GlaxoWellcome Stevenage.  
*"Apolipoprotein E expression by neurons surviving excitotoxic stress."*
- 1997 Oxford University, Department of Human Anatomy:  
*"Dual specificity phosphatases: molecular and functional analysis."*
- 1996 The third TEL AVIV University Conference on Alzheimer Disease  
*" Effects of apolipoprotein E isoforms on axonal growth and synapse formation in vitro"*
- 1996 Centre medical Universitaire (CMU) Geneva:  
*"Dual activity Thre/Tyr phosphatases MKP1, MKP3 and MKPX"*
- 1996 3rd Verbier Neural Workshop: Neurodegenerative Diseases  
*"Alzheimer's disease, from human genetics to animal models"*
- 1994 Center for Neurobiology and Behaviour, Columbia University New York  
*"Kainic acid treatment induces the expression of SCG10 and MKP1 in rat hippocampus."*
- 1992 5th Swiss Workshop of Methodology in Receptor Research :  
*" 5HT1B, 5HT5, and 5HT6: cloning, coupling with second messengers and pattern of expression in the nervous system"*

EFO-231

04.09.2003



Journal of  
Hepatology

www.elsevier.com/locate/jhep



Journal of Hepatology 42 (2005) 833–841

# Cloning and characterization of hepaCAM, a novel Ig-like cell adhesion molecule suppressed in human hepatocellular carcinoma

Mei Chung Moh, Lay Hoon Lee, Shali Shen\*

Laboratory of Hepato-Oncogenetics, Department of Physiology, Faculty of Medicine, National University of Singapore,  
2 Medical Drive, Singapore 117597

**Background/Aims:** Previously, we reported on gene HEPN1 that was silenced in hepatocellular carcinoma (HCC) and its capability of arresting cell growth. In this study, we identified another novel gene hepaCAM from the liver, which contains the full-length HEPN1 on its antisense strand in the 3'-noncoding region, and assessed its expression, characteristics and functions in HCC.

**Methods:** Full-length hepaCAM cDNA was isolated by rapid amplification of cDNA ends. The gene expression was examined by semi-quantitative RT-PCR in 23 paired HCC liver specimens and 5 HCC cell lines. Transfection studies, coupled with immunocytochemistry, cellular interaction analyses, colony formation and microtetrazolium assay, were employed to elucidate the localization and functions of hepaCAM.

**Results:** The expression of hepaCAM decreased in 20/23 of HCC samples and was undetectable in 5 HCC cell lines tested. The gene product consisting of 416 amino acids displayed the typical structure of Ig-like cell adhesion molecules. The protein was glycosylated and predominantly localized on the cytoplasmic membrane. When re-expressed in HepG2, hepaCAM accelerated cell spreading ( $P < 0.001$ ), increased cell motility ( $P = 0.0011$ ), reduced colony formation ( $P = 0.0022$ ), and inhibited cell growth ( $P < 0.001$ ).

**Conclusions:** Gene hepaCAM, frequently silenced in HCC, encodes an Ig-like transmembrane glycoprotein and is involved in cell adhesion and growth control.

© 2005 European Association for the Study of the Liver. Published by Elsevier B.V. All rights reserved.

**Keywords:** Hepatocellular carcinoma; hepaCAM; Ig-like cell adhesion molecule; Cell growth arrest; Cell-matrix interaction; HEPN1

## 1. Introduction

Cell adhesion is crucial not only for the formation and maintenance of cellular architecture but also for the normal biological processes including adhesion, migration, proliferation and survival [1]. Such specialized recognition and adhesion are mediated by cell adhesion molecules (CAMs) expressed on the cell surface. Generally classified into cadherins [2,3], selectins [4], integrins [5], and immunoglobulin superfamily (IgSF) [6], these glycoproteins recognize and interact either with other cell adhesion molecules on the adjacent cell surface or with proteins

deposited in the extracellular matrix. In addition to the adhesive properties of these molecules, an exciting concept that has emerged from recent cell biological research is that cell adhesion complexes are not simply static architectural entities. Rather, they are dynamic units that are critical in modulating cytoplasmic signaling cascades by capturing and integrating signals from the extracellular environment [2].

Cell organization and tissue architecture of the liver are well defined. Approximately, 80% of the adult liver consists of hepatocytes that are arranged as single-cell anastomosing plates extending from the portal region of the liver lobule towards the central vein [7]. Proper liver architecture is crucial for hepatic function [8] and is commonly disrupted in disease/injury state, including hepatitis, cirrhosis [9] and hepatocellular carcinoma [10]. Disruption of normal cell-cell adhesion in transformed cells may contribute to tumor cells' enhanced

Received 24 September 2004; received in revised form 6 January 2005;  
accepted 15 January 2005; available online 7 April 2005

\* Corresponding author. Tel.: +65 6874 6406; fax: +65 6778 8161.

E-mail address: phsssl@nus.edu.sg (S. Shen).

0168-8278/\$30.00 © 2005 European Association for the Study of the Liver. Published by Elsevier B.V. All rights reserved.  
doi:10.1016/j.jhep.2005.01.025



migration and proliferation, leading to invasion and metastasis. Although the underlying mechanism of how these phenotypes are resulted remains elusive, such disruption has been related to inactivation of cadherin, or the catenin family members, and activation of signaling pathways that prevent the assembly of adherens junctions [11].

Extensive studies have shown that the disruption of cell adhesion plays a causal role in tumor progression and metastasis [12]. Alterations of several IgSF tumor suppressors have been implicated in tumor malignancies. One such intriguing Ig-containing protein is the neural cell adhesion molecule (NCAM), a cell surface sialoglycoprotein, which is involved in neural development, signal transduction and synaptic plasticity and is downregulated during tumorigenesis [13–17]. A correlation between reduced NCAM expression and poor prognosis has been reported in several cancer types, including gastrointestinal neoplasia, colorectal cancer, and pancreatic cancer [18–20]. Another IgSF adhesion protein implicated in carcinogenesis is the carcinoembryonic antigen cell adhesion molecule-1 (CEACAM1), an epithelial cell adhesion molecule, which is frequently downregulated in liver, colorectal and prostate cancers [21–24]. Consistently, ectopic restoration of its expression in colorectal and prostate carcinoma cells significantly suppressed their tumorigenicity *in vitro* and *in vivo* [24–26], suggesting that CEACAM1 functions as a tumor suppressor gene. Moreover, CEACAM1 is an angiogenic factor and an effector of vascular endothelial growth factor in endothelial cells; and has been implicated in cell invasion and metastasis [27,28].

In our previous study, examining genes associated with human hepatocellular carcinoma (HCC) by suppression subtractive hybridization, we identified a novel gene, HEPN1, frequently silenced in HCC [29]. Interestingly, an updated BLAST search revealed that an mRNA sequence in the database (GenBank AF834419), encoding a partial open reading frame (ORF) at the 5' terminus, contained the entire antisense strand of HEPN1 in its 3' noncoding region. This finding led us to isolate a new gene with a full-length cDNA approximately 3.2 kb. The gene encodes a putative Ig-like cell adhesion molecule with 416 amino acids, designated as hepaCAM. In this report, we demonstrate the expression, characteristics and functions of hepaCAM in hepatocellular carcinoma.

## 2. Materials and methods

### 2.1. Isolation of hepaCAM full-length cDNA

Rapid amplification of cDNA ends was performed with the Human Liver Marathon-Ready™ cDNA Kit (Clontech) according to the manufacturer's instructions. The gene-specific primer (QSP, 5'-GCTAGGCACTCTGCTGGATGCTAGTA-3') designed at the 5'-end on the antisense strand of HEPN1 was used with the adapter primer 1 (provided) to amplify the full-length cDNA of hepaCAM. The cDNA was cloned and sequenced.

### 2.2. Liver specimens and cell lines

A total of 23 paired liver specimens and 6 normal liver tissues were surgically collected at the No. 3 Hospital of Chongqing in China through Dr. Yang Xiaodong. The final diagnosis of HCC was confirmed and classified by histological examination. Five human HCC cell lines, HepG2, Hep3B, Huh7, SK-Hep1 and PLC-5, were maintained in the recommended conditions.

### 2.3. RT-PCR

Semi-quantitative RT-PCR reactions were performed with the OneStep RT-PCR kit (Qiagen) while real-time RT-PCR was performed with the LightCycler RNA Amplification Kit SYBR Green 1 (Roche). A forward primer (5'-TGACAGCTGCATGGTGGAGA-3') and a reverse primer (5'-TCTGGTTTCAGCGGTCATCA-3') were used to generate a hepaCAM fragment of 235 bp from 0.2 µg of DNase-treated total RNA. Beta-actin or GAPDH was included as control.

### 2.4. Plasmid construct

The open reading frame of hepaCAM was generated by PCR from the full-length cDNA with the forward primer 5'-GAAGCTT(HindIII)-CAAAATGGAGAGAGAAAGGGGAGCC-3' and the reverse primer 5'-AGGATCC(BamHI)-GGCCGAGGCGCTGATCTCCACC-3'. The PCR product was cloned into the HindIII/BamHI restriction sites of pDNA6/V5-His (Invitrogen). The construct, namely hepaCAM-V5, facilitated the expression of hepaCAM-V5 fusion protein and the detection by anti-V5 antibody.

### 2.5. Transfection

Transient transfections were carried out with Lipofectamine Plus (Invitrogen). Hep3B and HepG2 cells grown on coverslips were transfected with either hepaCAM-V5 or pDNA6/V5-His (pDNA6) vector for 48 h before immunocytochemistry. Stable transfections were performed on HepG2 cells. Transfected cells were selected in the presence of 10 µg/ml of blasticidin (Invitrogen) for 3 weeks and then cloned.

### 2.6. Immunocytochemistry

Cells cultured on coverslips were washed with PBS, fixed with 2% paraformaldehyde, and permeabilized with 0.2% Triton-X 100. Nonspecific sites were blocked in 10% normal goat serum (Santa Cruz). Protein expression of hepaCAM was detected using mouse anti-V5 antibody (Invitrogen) diluted at 1:200, biotin-conjugated goat anti-mouse IgG antibody (3 µg/ml), and subsequently streptavidin-fluorescein (15 µg/ml). Fluorescence was visualized by Fluorescence Microscope and Confocal Microscope LSM 510 (Carl Zeiss).

### 2.7. Western analysis

Total protein (50 µg) from HepG2 or liver tissue was resolved by SDS-PAGE, transblotted onto membrane, and detected by either rabbit anti-hepaCAM polyclonal antibody (generated following the procedure described in the Current Protocol) or mouse anti-V5 monoclonal antibody. The membranes were stripped and reprobed with mouse anti-GAPDH antibody (Chemicon) to assess loading quantity.

### 2.8. Deglycosylation

Cell lysate was deglycosylated with peptide N-glycosidase F (PNGase F) (New England Biolabs) according to the manufacturer's instructions. Equal amount of cell lysate without PNGase F treatment served as control. These samples were then subjected to western analysis.

## 2.9. Cell spreading

Cells were seeded in plates coated with 10 µg/ml-fibronectin (Santa Cruz) and incubated under standard conditions. Cell morphology was observed by microscopy (Carl Zeiss). Unspread cells were defined as round cells, while spread cells were defined as cells with extended processes [30]. The percentage of cells demonstrating spread morphology was quantified in 10 randomly selected fields (>60 cells/field).

## 2.10. Matrigel invasion assay

Cell migration was assessed using the transwell chambers with 8-µm pore size membranes coated with matrigel (BD Biosciences) in 24-well plates. Cells ( $5 \times 10^4$ ) were loaded into the upper volume of the chambers and allowed to migrate through the membrane for 24 h. Non-migrated cells were removed with a cotton swab, and the migrated cells were harvested by trypsinizing the lower surface of the membrane and collected into new 24-well plate. The migration activity was quantified by blind counting of the migrated cells in 10 randomly selected microscopic fields (>40 cells/field).

## 2.11. Wound closure assay

Cell motility was also assessed by the wound healing experiment on monolayer cells. Cells were seeded in 35-mm culture plates at high density and allowed to form monolayers overnight. Wounds were made by pipette tip on confluent cells and allowed to be healed by cell migration for 24 h. The changes in diameter ( $D$ ) of each wound were measured by microscopy and computed into ratio ( $D_{24}/D_{initial} \times 100\%$ ) to represent wound closure.

## 2.12. Colony formation

HepG2 cells transfected with either hepaCAM-V5 or vector pcDNA6 were selected in 10 µg/ml of blasticidin (Invitrogen) for 3 weeks without trypsinization while medium was refreshed every 2 days. The cell colonies formed at the end of experiment were visible, and the size and thickness of the colonies were analyzed by microscopy. The number of colonies was counted in 10 randomly selected fields.

## 2.13. Growth curve

The growth rate of HepG2 stable cell lines was monitored for 5 days. Cells were seeded in triplicates and cultured under standard conditions. At every 24 h, cell viability was determined by MTT assay. The growth rate of each cell line was presented as folds of increase in cell viability against the respective base line obtained on the day of seeding cells.

## 2.14. Bioinformatics and statistical analysis

Sequence analyses were carried out through database searches (facilitated by the NCBI, Ensembl and ExPASy). Mann-Whitney test was performed to compare two means of samples with small sample size ( $n=6$ ). Fisher's exact test was used to assess the correlation between two parameters. Nonparametric ANOVA was performed to compare the differences between more than two means. Software InStat 3.0 (GraphPad) was employed and  $P < 0.05$  was considered as significant.

## 3. Results

### 3.1. Identification of hepaCAM

As illustrated in Fig. 1, the cDNA sequence AL834419 (GenBank) containing the antisense strand of HEPN1 in its 3'-noncoding region was deficient in the 5'-noncoding region. The gene specific primer (GSP) at the 5'-end of HEPN1 antisense strand and the adaptor primer (AP1) enabled us to isolate a new gene, hepaCAM, from a human normal liver cDNA library. Gene hepaCAM was mapped to human chromosome 11q24 and its genomic DNA sequence contained 7 exons ranging in sizes from 71 to 2252 bp. The full-length cDNA sequence of hepaCAM (3244 bp) has been submitted to the GenBank (AY047587).

### 3.2. Suppression of hepaCAM in HCC

Semi-quantitative RT-PCR revealed that hepaCAM was expressed at a similar level in all the normal liver tissues tested (Fig. 2A). To evaluate if hepaCAM expression was downregulated in HCC, we examined hepaCAM mRNA levels in 23 paired liver samples from HCC patients using a pair of hepaCAM specific primers that were not associated with the HEPN1 sequence. The results showed that hepaCAM was reduced in 87% (20/23) of HCC tissues (Fig. 2B). The expression of hepaCAM was not detectable when evaluated in 5 human HCC cell lines HepG2, Hep3B,

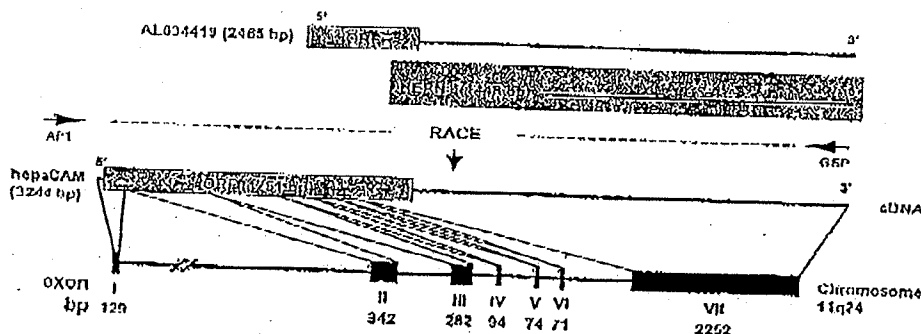


Fig. 1. Molecular cloning of hepaCAM. (A) Reconstitution scheme of hepaCAM. The full-length cDNA of hepaCAM was isolated from normal human liver cDNA library by RACE. A forward primer on the adaptor (AP1) and a gene specific primer (GSP, the reverse primer) at the 5'-end of HEPN1 antisense strand were used in the RACE reaction. The cDNA lengths of hepaCAM, HEPN1 and sequence AL834419 are given in the brackets. The indications of 5' and 3' correspond to the orientations of the cDNA. The genomic DNA of hepaCAM mapped to human chromosome 11q24 contains 7 exons indicated as I–VII and accompanied by their respective length in base pairs (bp). [This figure appears in colour on the web.]

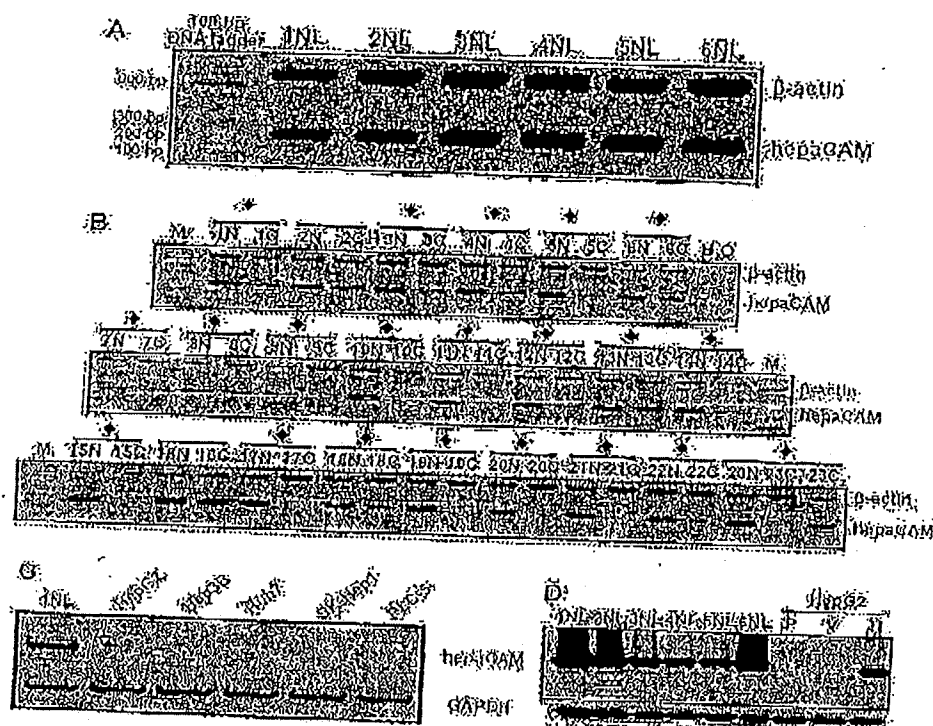


Fig. 2. Expression of hepaCAM in liver specimens and HCC cell lines. (A) Expression of hepaCAM in normal liver tissues. Semi-quantitative RT-PCR was performed to determine the mRNA expression of hepaCAM in 6 normal liver tissues obtained from 6 individuals. Two pairs of gene specific primers were included in one RT-PCR reaction to generate the fragments of genes  $\beta$ -actin (720 bp, as the internal control) and hepaCAM (235 bp), respectively. The samples are labeled from 1 to 6; NL, normal liver. (B) Expression of hepaCAM in 23 HCC patients. Semi-quantitative RT-PCR products were analyzed by gel electrophoresis. \*, samples that show clear differences in hepaCAM expression; N, non-tumor liver tissue; C, HCC liver tissue;  $\beta$ -actin, internal control. Patient 23 had two HCC nodules (C<sub>1</sub> and C<sub>2</sub>) in the liver. (C) Expression of hepaCAM in five hepatic cell lines. Semi-quantitative RT-PCR was used to amplify hepaCAM mRNA and GAPDH mRNA (internal control). The expression level of hepaCAM in 5 HCC cell lines, HepG2, Huh7, SK-Hep1 and PLC-5, was compared to that in the normal liver tissue NL. (D) Protein levels of hepaCAM in normal liver tissues and HepG2 cells. Western analysis with rabbit anti-hepaCAM polyclonal antibody revealed the endogenous hepaCAM protein levels in 6 normal liver tissues and the exogenous protein in hepaCAM-transfected HepG2 cells (H). No hepaCAM protein was detectable in both the parental (P) and the vector-transfected (V) HepG2 cells. GAPDH protein level indicates the loading quantity.

Huh7, SK-Hep1 and PLC-5 (Fig. 2C). Furthermore, western analysis with anti-hepaCAM polyclonal antibody confirmed the protein expression of hepaCAM in all the normal liver tissues, as well as in HepG2 cells transfected with hepaCAM, but neither in the parental HepG2 cells nor in the cells transfected with vector alone (Fig. 2D). These data implied the association between the loss of hepaCAM and hepatocarcinogenesis. No correlations between hepaCAM and the clinicopathologic parameters could be detected. This could be due to the high rate of hepaCAM suppression in the HCC samples tested (Table 1).

### 3.3. Characterization of hepaCAM protein sequence

Gene hepaCAM encoded a 46-kDa protein of 416 amino acids consisting of an extracellular region, a transmembrane segment, and a cytoplasmic tail (Fig. 3A). The extracellular region comprised a signal

Table 1  
Correlation between hepaCAM suppression and the clinicopathologic parameters in 23 HCC patients

Parameters	hepaCAM suppression	Unchanged hepaCAM	Suppression rate (%)	P
Total number	20	3	87	
Sex				
Male	16	2	89	NS
Female	4	1	80	NS
Grade				
Well	3	0	100	NS
Moderate	12	2	86	NS
Poor	5	1	83	NS
Cirrhosis	16	3	84	NS
Hepatitis virus				
HBV	18	2	90	NS
HCV	3	0	100	NS
HBV+HCV	2	0	100	NS

Grade, histological differentiation of HCC; NS, not significant; P was revealed by the Fisher's exact test.

peptide and 2 Ig domains (Ig-like and C2 domains) as predicted by SignalP [31] and SMART [32], respectively. Two cysteine residues flanking the C2 domain contributed to the formation of intrachain disulfide-linked loop. Six *N*-glycosylation sites were identified in the extracellular region, which may contribute to the glycosylation of hepaCAM protein. The transmembrane segment was found to contain a prokaryotic membrane lipoprotein lipid attachment site (LLVTLVTVAC). At the cytoplasmic tail, two potential class III PDZ domain-binding motifs were predicted. Overall, the structure of hepaCAM closely resembles Ig-like cell adhesion molecules.

### 3.4. Deglycosylation of hepaCAM protein

The molecular weight of the epitope-tagged hepaCAM shown by western analysis was approximately 75 kDa, larger than the predicted size (46 kDa). The six *N*-glycosylation sites identified on hepaCAM protein within the extracellular region (Fig. 3B) implied that hepaCAM protein might be glycosylated. The cleavage of *N*-linked glycans on hepaCAM by PNGase F indeed shifted the molecular weight from 75 to 60 kDa (Fig. 3C), indicating hepaCAM a glycoprotein. Noticeably, the molecular weight of the deglycosylated protein was still higher than the predicted one, suggesting the involvement of additional post-translational modifications.

### 3.5. Cellular localization of hepaCAM

Two hepatic cell lines Hep3B and HepG2, in which hepaCAM was undetectable (Fig. 2C), were transiently transfected with hepaCAM-V5. Immunofluorescence staining with anti-V5 antibody showed that hepaCAM was scattered in the cytoplasm, absent in the nucleus and predominantly localized on the plasma membrane of both Hep3B and HepG2 cells (Fig. 4A). Interestingly, the cellular localization of hepaCAM appeared to be cell density-dependent in HepG2 with stable transfection. In well-spread cells (Fig. 4B upper), hepaCAM was distributed in the cytoplasm and at the cell surface protrusions that were about to make cell contacts. In confluent cells (Fig. 4B lower), hepaCAM was predominantly localized on the cytoplasmic membrane, particularly in the areas of cell-cell contacts.

### 3.6. Evaluation of stable transfection

Two clones stably transfected with vector (V1 and V2) and 3 clones with hepaCAM-V5 (H1, H2 and H3) were screened. Western analysis showed that hepaCAM was absent in the vector clones V1 and V2, and expressed in 2 (among 3) hepaCAM clones H1 and H3 (Fig. 5A). Real-time RT-PCR showed that hepaCAM was expressed in clones H1 and H3 but not overexpressed when compared to the normal liver tissues, and was expectedly absent in clones V1, V2 and H2 (Fig. 5B). Immunofluorescence staining and confocal microscopy confirmed the establishment of cell clones (Fig. 5C). Clones V1, V2, H1 and H3 were therefore selected for the downstream functional exploration of hepaCAM.

### 3.7. Cell-matrix interaction and cell motility modulated by hepaCAM

As hepaCAM displayed the typical structure of cell adhesion molecules, we evaluated the adhesive properties of hepaCAM on the stable HepG2 clones through cell aggregation and spreading assays. Although hepaCAM did not clearly change cell aggregation (data not shown), it was

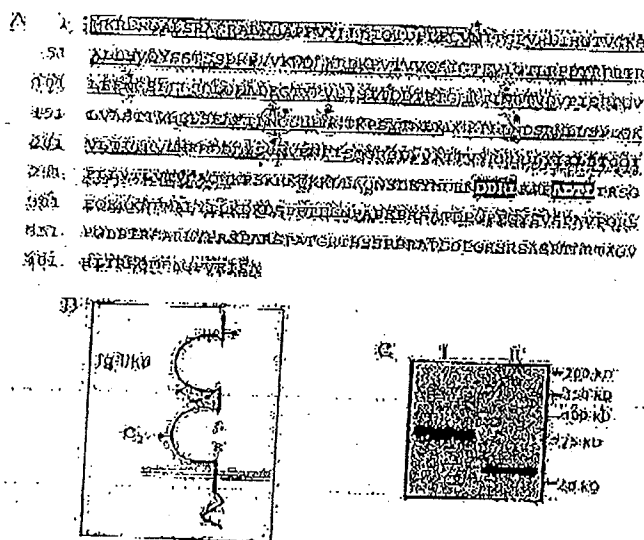


Fig. 3. The characteristics of hepaCAM protein sequence. (A) Predicted amino acid sequence of human hepaCAM. The fragment highlighted in the box is the putative signal peptide (24 amino acids). The regions underlined with solid lines are the two immunoglobulin-like (Ig-like) domains (103 and 66 amino acids, respectively) while the one underlined with dashed line is the transmembrane domain (23 amino acids). Two cysteine residues (marked underneath the '●') are identified in the second Ig-like domain, which may be needed for the formation of the disulfide bond in the domain. Six asparagines (marked underneath the '★') are in the extracellular region, which represent the potential *N*-linked glycosylation sites. The class III PDZ domain binding motifs (in the inverted shades) are present in the cytoplasmic region. (B) Illustration of the secondary structure of hepaCAM protein. hepaCAM owns the typical structure of proteins in the immunoglobulin superfamily, including an extracellular segment consisting of an *N*-terminal-proximal Ig-like domain and a membrane-proximal C<sub>2</sub>-type Ig-domain with a disulfide bond formed between two cysteine residues (S S), a transmembrane region, and a cytoplasmic tail. The six putative *N*-linked glycosylation sites are indicated by the signs of '★'. (C) Deglycosylation of hepaCAM. HepG2 cells transfected with hepaCAM were lysed and treated with (lane II) or without (lane I) peptide *N*-glycosidase F. The cell lysates were resolved by SDS-PAGE and subjected to western blotting with anti-V5 antibody.

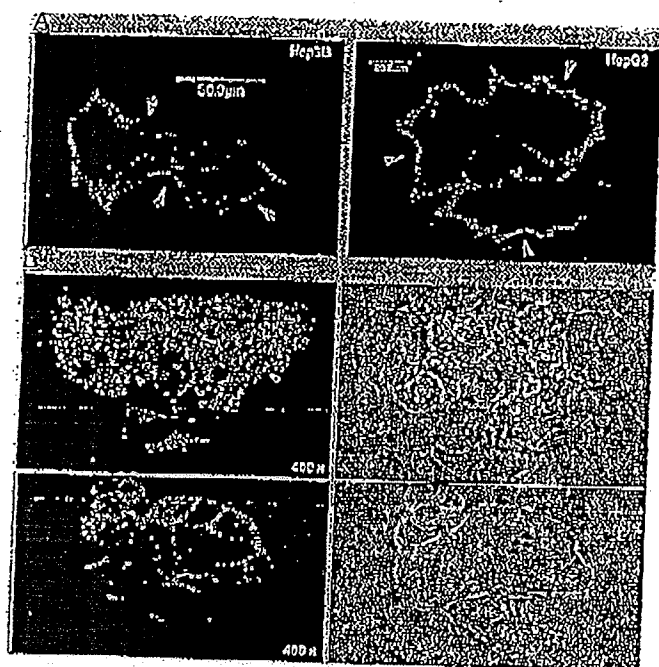


Fig. 4. Cellular localization of hepaCAM. (A) Through transient transfection and immunocytochemistry, hepaCAM protein was localized in 2 HCC cell lines. Fused with V5 in vector pcDNA6/V5-His, hepaCAM was transfected into Hep3B and HepG2 cells. Anti-V5 antibody was used for immunostaining to detect the expression and localization of hepaCAM. Confocal microscopy revealed that hepaCAM was scattered in the cytoplasm and predominantly localized on the cell membrane (arrows). (B) The localization of hepaCAM in HepG2 cells with stable transfection was cell density-dependent. Upper panel, well-spread cells with surface protrusions (arrow heads); lower panel, confluent cells with clear cell-cell contacts. [This figure appears in colour on the web.]

capable of modulating cell-matrix adhesion significantly (Fig. 6A). About 50% and 90% of the cells from both clones H1 and H3 exhibited spread morphology at 30 min and 2 h of incubation, respectively (Fig. 6B). In contrast, the majorities of the cells from clones V1 and V2 remained round at the same time points. The number of cells showing spread morphology from clones H1 and H3 was about 5 folds higher than that from the control clones V1 and V2 ( $P < 0.001$ ). Furthermore, HepG2 cell motility was increased ( $P = 0.0011$ ) when transfected with hepaCAM as determined by matrigel invasion (Fig. 7A) and wound healing assays in culture dish (Fig. 7B). These results indicate that hepaCAM may be involved in cell and extracellular matrix interactions.

### 3.8. Antiproliferative effect of hepaCAM

Many Ig-like adhesion molecules, such as NCAM-1 [14], TSLC-1 [33], and OPCML [34], are known as tumor suppressors exhibiting antiproliferative effects. To examine

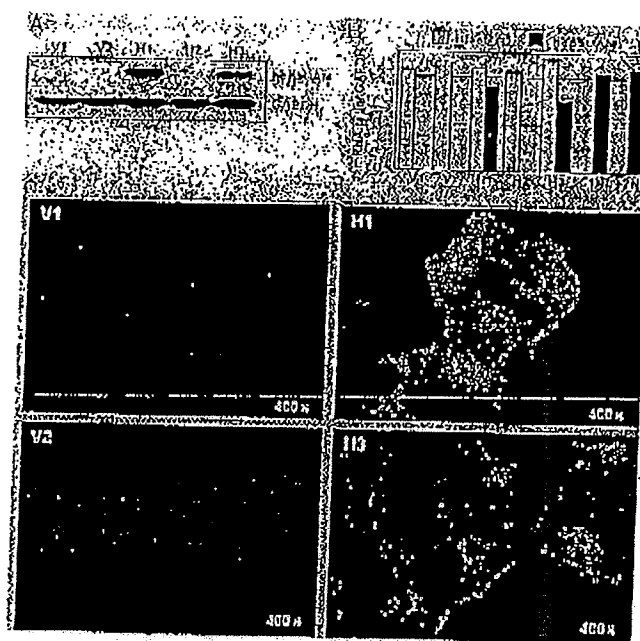


Fig. 5. Stable transfection of hepaCAM in HepG2. HepG2 cells stably transfected with vector or hepaCAM-V5 construct were cloned. (A) Western analysis. Anti-V5 antibody was used in the western analysis to evaluate the protein levels of hepaCAM in two clones transfected with vector alone (V1 and V2) and three clones transfected with hepaCAM-V5 (H1, H2, and H3). The membrane was stripped and reprobed with anti-GAPDH antibody for loading control. (B) Real-time RT-PCR analysis. The mRNA levels of blastocidin resistant gene (Blast\_r) and hepaCAM were determined in all the clones and two normal liver tissues (INT, and 2NL), and converted into ratio against GAPDH mRNA levels. (C) Confocal microscopy. Immunofluorescence staining through anti-V5 antibody was used to visualize hepaCAM protein in both cells from the control clones V1 and V2 and cells from the clones expressing hepaCAM (H1 and H3). 400 $\times$ , magnification. [This figure appears in colour on the web.]

the involvement of hepaCAM in cell growth control, colony formation was carried out while growth rate was determined in stable HepG2 clones. The results showed that the number of colonies was reduced by 10 folds in the cells transfected with hepaCAM ( $P = 0.0022$ , Fig. 8A), and the growth rate was decreased by 14 folds ( $P < 0.001$ , on day 5, Fig. 8B) in cells expressing hepaCAM (H1 and H3). No clear cell death was observed in the course of examining growth arrest, suggesting that hepaCAM inhibits cell growth through suppressing proliferation rather than inducing apoptosis.

### 4. Discussion

We have identified hepaCAM as a new Ig-like adhesion molecule. The novel protein displays the typical structure of the adhesion molecules in immunoglobulin superfamily (IgSF), including two extracellular Ig-like domains, a single transmembrane region, and a cytoplasmic tail [6].

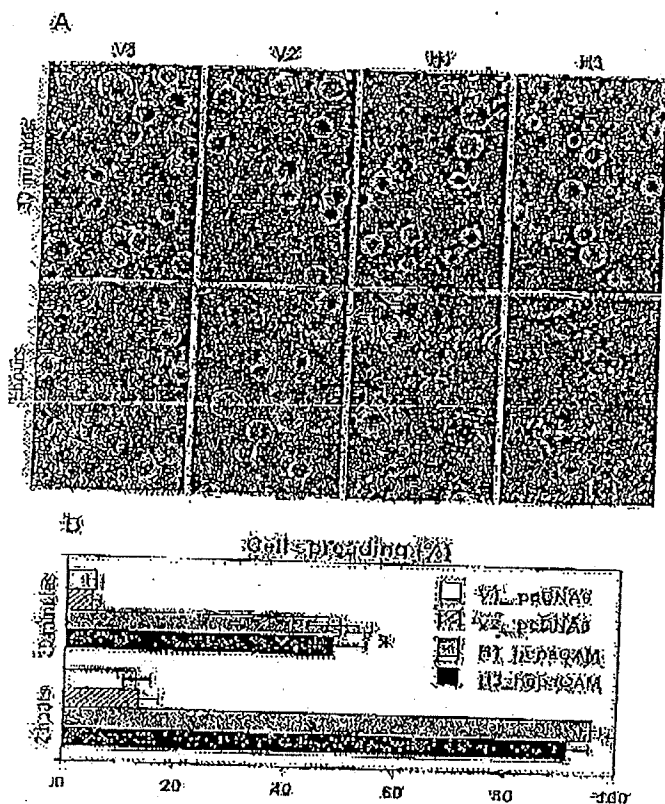


Fig. 6. Modulation of cell-matrix adhesion by hepaCAM. (A) Cell morphology. HepG2 clones transfected with vector alone (V1 and V2) and expressing hepaCAM-V5 (H1 and H3) were allowed to spread on fibronectin-coated plates for 30 min or 2 h. The microscopic photos were taken under 200 $\times$  magnification. (B) The percentage of cell spreading. At 30 min or 2 h after plating, total number of cells and cells showing spread morphology were counted in ten randomly selected fields (>60 cells per field), and the percentage of cell spreading was then computed. The data represent means  $\pm$  SD ( $n=6$ ). \* $P<0.001$  as assessed by ANOVA.

The structure of hepaCAM is similar to that of adhesion molecules JAMs, CAR, and ESAM, which are known to be involved in cellular interactions. Experimentally, we have demonstrated that hepaCAM protein is glycosylated and predominantly localized on plasma membrane, particularly in the areas of cell–cell contacts when cells are confluent. Such distribution is also shown with JAMs, CAR, and ESAM. Moreover, revealed by cell spreading and motility assays, hepaCAM is capable of modulating cell–matrix interactions, further supporting hepaCAM to be an adhesion molecule.

Intriguingly, our data suggest that hepaCAM may be a tumor suppressor in human hepatocellular carcinoma. Firstly, we show that hepaCAM is expressed in all normal and non-tumorous liver tissues, but suppressed in 87% (20/23) of HCC patients and 100% (5/5) of HCC cell lines, i.e. when hepatocytes have become cancerous, indicating that loss of hepaCAM expression is associated

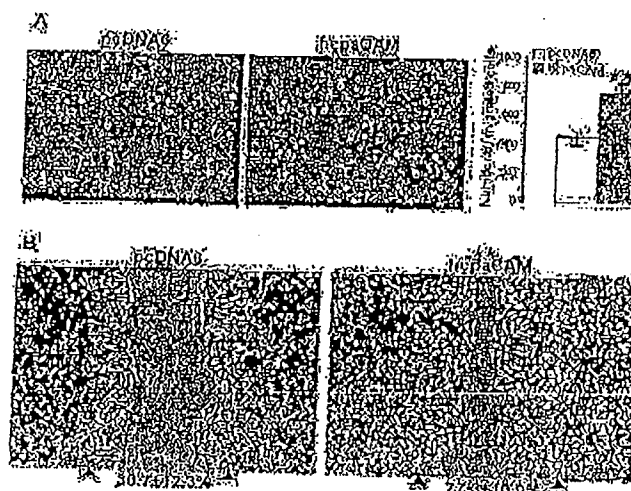


Fig. 7. Modulation of cell motility by hepaCAM. (A) Matrigel invasion assay. Cell migration was examined by using the transwell chambers with 8- $\mu$ m pore size membranes coated with matrigel. HepG2 cells stably transfected with either pcDNA6 vector or hepaCAM-V5 were allowed to migrate through the membrane for 24 h. The migrated cells were harvested into new 24-well plate and viewed by microscopy (100 $\times$ ). The migration was quantified by blind counting of the migrated cells in 10 randomly selected fields and represented as mean  $\pm$  SD ( $n=6$ ) by the bar graph. (B) In vitro wound healing assay. Wounds were made by pipette tip on confluent HepG2 cells stably transfected with either pcDNA6 vector alone (left) or hepaCAM-V5 (right) and allowed to be healed by cell migration for 24 h. The diameters of wounds were measured by microscopy (200 $\times$ ) at 0 h and 24 h after wounding. Arrow heads show the diameters of the initial wounds. Changes in diameter were computed into ratio (mean  $\pm$  SD%,  $n=6$ ) to represent wound closure. \*\* $P=0.0011$  as assessed by Mann–Whitney test.

with hepatocarcinogenesis. Secondly, the accelerated cell–matrix adhesion mediated by hepaCAM raises the possibility that loss of hepaCAM may ultimately lead to the disruption of liver tissue architecture by the loss of a tumor cell's ability to communicate with its extracellular environment. Thirdly, transfection studies revealed that hepaCAM reduced cell colony formation and inhibited cell growth in HCC cell line HepG2 through suppression of cell proliferation. The frequent loss of hepaCAM expression in HCC together with the antiproliferative effect of hepaCAM meets the most important criteria widely used to define tumor suppressor.

In addition, hepaCAM is mapped to the human chromosome 11q24. Molecular genetic and cytogenetic studies have indicated that the long arm of chromosome 11 is one of the most common targets for chromosomal aberrations during the progression of human malignancies. Tumor suppressor genes encoding cell adhesion molecules of the Ig superfamily have been identified on 11q22–qter. An Ig-like adhesion molecule TSLC1 is a tumor suppressor at 11q23 and its expression through promoter hypermethylation has been reported in the development of many human cancers such as cancers of the lung, cervix, breast and prostate [35]. However, no studies have reported

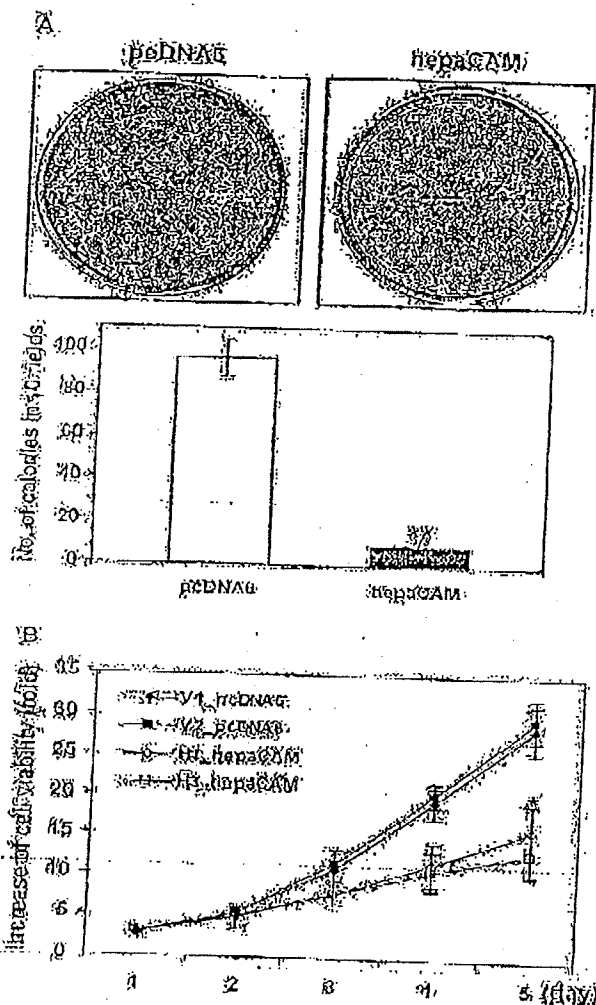


Fig. 8. Inhibition of cell growth by hepaCAM. (A) Colony-formation. HepG2 cells transfected with vector (pcDNA6) or hepaCAM-V5 construct (hepaCAM) were selected with blastfiscidin for 3 weeks. The cell colonies formed at the end of the experiments were visible (upper panel) and the size and the thickness of the colonies were observed by microscopy. The number of colonies was counted in 10 randomly selected fields and represented by the bar graph (means  $\pm$  SD,  $n=6$ ),  $**P=0.0022$  as assessed by Mann–Whitney test. (B) Cell growth curve. The growth rate of the cells from clones IIT and H3 (stably transfected with hepaCAM-V5) was compared to that of the cells from V1 and V2 (stably transfected with vector alone) for 5 days by microtetrazolium (MTT) assay. Data represent means  $\pm$  SD ( $n=6$ ),  $*P<0.001$  (on day 5) as assessed by ANOVA.

the loss of heterozygosity (LOH) of chromosome 11q in HCC and the mode of hepaCAM gene silencing is yet to be understood.

In conclusion, we have identified a novel gene hepaCAM that encodes an Ig-like cell adhesion molecule. Gene hepaCAM is found frequently silenced in human hepatocellular carcinoma and the gene product is shown to be a transmembrane glycoprotein. When re-expressed in

HepG2, hepaCAM is capable of mediating cell-matrix adhesion and cell motility, and exhibits antiproliferative effect. This study suggests that hepaCAM is a new Ig-like cell adhesion molecule which may play roles in cell-matrix interaction and cell growth regulation.

#### Acknowledgements

The study was supported by the National Medical Research Council (NMRC/0598/2001) and the Biomedical Research Council (Project No. 01/1/21/19/162) of Singapore. We thank Miss Asha Reka Das for her assistance whenever and wherever needed.

#### References

- [1] Edelman GM. Cell adhesion molecules in the regulation of animal form and tissue pattern. *Annu Rev Cell Biol* 1986;2:81–116.
- [2] Rosales C, O'Brien V, Kornberg L, Julliano R. Signal transduction by cell adhesion receptors. *Biochim Biophys Acta* 1995;1242:77–98.
- [3] Wesseling J, van der Valk SW, Hilkens J. A mechanism for inhibition of E-cadherin-mediated cell-cell adhesion by the membrane-associated mucin epistatin/MUC1. *Mol Biol Cell* 1996;7:565–577.
- [4] Todder TF, Steeber DA, Pizenet P. L-selectin deficient mice have impaired leukocyte recruitment into inflammatory sites. *J Exp Med* 1995;181:2259–2264.
- [5] Hynes RO. Targeted mutations in cell adhesion genes: what have we learned from them? *Dev Biol* 1996;180:402–412.
- [6] Williams AF, Barclay AN. The immunoglobulin superfamily—domains for cell-surface recognition. *Annu Rev Immunol* 1993;6:381–405.
- [7] Ross M, Kaya GI, Pawlina W. Digestive System III: Liver, Gallbladder, and Pancreas. In: *Histology: a text and atlas*. 532. Baltimore: Lippincott Williams and Wilkins; 2002 p. 532–47.
- [8] Kmiec Z. Cooperation of liver cells in health and disease. *Adv Anat Embryol Cell Biol* 2001;161:1–151.
- [9] Sherlock S, Dooley J. Hepatic cirrhosis. In: *Diseases of liver and biliary system*. Oxford: Blackwell Science; 1997 p. 371–82.
- [10] Yoshidome S, Tanabe G, Yoshida A, Ueno S, Hatanouchi M, Mitna S, et al. Risk prediction using histology of noncancerous liver before hepatic resection for hepatocellular carcinoma. *Hepatogastroenterology* 2001;48:518–522.
- [11] Ben-Ze'ev A, Geiger B. Differential molecular interactions of  $\beta$ -catenin and plakoglobin in adhesion, signaling and cancer. *Curr Opin Cell Biol* 1998;10:629–639.
- [12] Hirohata S. Inactivation of the E-Cadherin-mediated cell adhesion system in human cancers. *Am J Pathol* 1998;153:333–339.
- [13] Williams EJ, Furness J, Walsh RS, Doherty P. Characterisation of the second messenger pathway underlying neurite outgrowth stimulated by FGF. *Development* 1994;120:1685–1693.
- [14] Krushel LA, Tai MH, Cunningham BA, Edelman GM, Crossin KL. Neural cell adhesion molecule (N-CAM) domains and intracellular signaling pathways involved in the inhibition of astrocyte proliferation. *Proc Natl Acad Sci USA* 1998;95:2592–2596.
- [15] Beggs HE, Soriano P, Maness PF. NCAM-dependent neurite outgrowth is inhibited in neurons from Fyn-minus mice. *J Cell Biol* 1994;127:825–833.
- [16] Beggs HE, Baragana SC, Hemperly JJ, Maness PF. NCAM140 interacts with the focal adhesion kinase p125(fak) and the SRC-related tyrosine kinase p59(fyn). *J Biol Chem* 1997;272:8310–8319.

- [17] Roun LC, Berezin V, Bock E. The neural cell adhesion molecule in synaptic plasticity and ageing. *Int J Dev Neurosci* 2000;18:193-199.
- [18] Fogar P, Basso D, Pasquali C, De Paoli M, Sperti C, Roveroni G, et al. Neural cell adhesion molecule (N-CAM) in gastrointestinal neoplasias. *Anticancer Res* 1997;17:1227-1230.
- [19] Roessler J, Srivatsan E, Moatamed F, Peters J, Livingston EH. Tumor suppressor activity of neural cell adhesion molecule in colon carcinoma. *Am J Surg* 1997;174:251-257.
- [20] Tezel B, Kawase Y, Takeda S, Oshima K, Nakao A. Expression of neural cell adhesion molecule in pancreatic cancer. *Pancreas* 2001;22:122-125.
- [21] Tanaka K, Hinoda Y, Takahashi H, Sakamoto H, Nakajima Y, Imai K. Decreased expression of biliary glycoprotein in hepatocellular carcinomas. *Int J Cancer* 1997;74:15-19.
- [22] Kleinerman DI, Tsimmos P, Lin SH, Pisters LL, Sherwood ER, Brooks T, et al. Consistent expression of an epithelial cell adhesion molecule (C-CAM) during human prostate development and loss of expression in prostate cancer: implication as a tumor suppressor gene. *Cancer Res* 1995;55:1215-1220.
- [23] Neumaier M, Paululat S, Chan A, Matthies P, Wagener C. Biliary glycoprotein, a potential human cell adhesion molecule, is down-regulated in colorectal carcinomas. *Proc Natl Acad Sci USA* 1993;90:10744-10748.
- [24] Heich JI, Luo W, Song W, Wang Y, Kleinerman DI, Van NT, et al. Tumor suppressive role of an androgen-regulated epithelial cell adhesion molecule (C-CAM) in prostate carcinoma cell revealed by sense and antisense approaches. *Cancer Res* 1995;55:190-197.
- [25] Hsieh JT, Bailey K, Pong RC, Wang X, Van NT, Lin SH. Structural analysis of the C-CAM1 molecule for its tumor suppression function in human prostate cancer. *Prostate* 1999;41:31-38.
- [26] Kunath T, Ordonez-garcia C, Turbide C, Beauchemin N. Inhibition of colonic tumor cell growth by biliary glycoprotein. *Oncogene* 1995;11:2375-2382.
- [27] Ergun S, Kilik N, Ziegeler G, Hansen A, Nollau P, Gotze J, et al. CEA-related cell adhesion molecule 1: a potent angiogenic factor and a major effector of vascular endothelial growth factor. *Mol Cell* 2000;5:311-320.
- [28] Brummer J, Elshinnecjad A, Flayah R, Schumacher U, Loning T, Damberger AM, et al. Interaction of the cell adhesion molecule CEACAM1 with integrin beta(3). *Am J Pathol* 2001;159:537-546.
- [29] Moh MC, Lee LH, Yang X, Shen S. HBPNI, a novel gene that is frequently down-regulated in hepatocellular carcinoma, suppresses cell growth and induces apoptosis in HepG2 cells. *J Hepatol* 2003;39:580-586.
- [30] Richardson A, Malik RK, Hildebrand JD, Parsons JT. Inhibition of cell spreading by expression of the C-terminal domain of focal adhesion kinase (FAK) is rescued by coexpression of Src or catalytically inactive FAK: a role for paxillin tyrosine phosphorylation. *Mol Cell Biol* 1997;17:6906-6914.
- [31] Nielsen H, Engelbrecht J, Bruunak S, von Heijne G. Identification of prokaryotic and eukaryotic signal peptides and prediction of their cleavage sites. *Protein Eng* 1997;10:1-6.
- [32] Letunic J, Goodstadt L, Dickens NJ, Doorks T, Schultz J, Mott R, et al. Recent improvements to the SMART domain-based sequence annotation resource. *Nucleic Acids Res* 2002;30:242-244.
- [33] Masuda M, Yagata M, Fukuhara H, Kuramochi M, Maruyama T, Nomiya A, et al. The tumor suppressor protein TSLC1 is involved in cell-cell adhesion. *J Biol Chem* 2002;277:31014-31019.
- [34] Sellar GC, Watt KP, Rablusz GJ, Stronach RA, Li L, Miller BP, et al. OPCML at 11q23 is epigenetically inactivated and has tumor-suppressor function in epithelial ovarian cancer. *Nat Genet* 2003;34:337-343.
- [35] Fletcher MT, Nobukuni T, Fukuhara H, Kuramochi M, Maruyama T, Sekiya T, et al. Identification of tumor suppressor candidate genes by physical and sequence mapping of the TSLC1 region of human chromosome 11q23. *Gene* 2001;273:181-189.



EPO-DS1

02.09.2003

THE JOURNAL OF BIOLOGICAL CHEMISTRY  
© 2005 by The American Society for Biochemistry and Molecular Biology, Inc.

Vol. 280, No. 20, Issue of July 22, pp. 27366–27374, 2005  
Printed in U.S.A.

## Structural and Functional Analyses of a Novel Ig-like Cell Adhesion Molecule, hepaCAM, in the Human Breast Carcinoma MCF7 Cells\*

Received for publication, January 24, 2005, and in revised form, May 24, 2005  
Published, JBC Papers in Press, May 25, 2005, DOI 10.1074/jbc.M500852200

Mei Chung Moh†, Chunli Zhang‡, Chunli Luo§, Lay Hoon Lee†, and Shali Shen†¶

From the †Department of Physiology, Faculty of Medicine, National University of Singapore, 2 Medical Drive, Singapore 117597, Republic of Singapore and ‡Department of Laboratory Diagnostics, Chongqing Medical University, Chongqing 400016, China

We have recently identified a novel gene, *hepaCAM*, in liver that encodes a cell adhesion molecule of the immunoglobulin superfamily. In this study, we examined the characteristics of *hepaCAM* protein and the relationship between its structure and function, in particular its adhesive properties. The wild-type and the cytoplasmic domain-truncated mutants of *hepaCAM* were transfected into the human breast carcinoma MCF7 cells, and the physiological and biological properties were assessed. Biochemical analyses revealed that *hepaCAM* is an N-linked glycoprotein phosphorylated in the cytoplasmic domain and that it forms homodimers through *cis*-interaction on the cell surface. The subcellular localization of *hepaCAM* appears density-dependent; in well spread cells, *hepaCAM* is distributed to cell protrusions, whereas in confluent cells, *hepaCAM* is predominantly accumulated at the sites of cell-cell contacts on the cell membrane. In polarized cells, *hepaCAM* is recruited to the lateral and basal membranes, and lacking physical interaction, *hepaCAM* is shown to co-localize with E-cadherin at the lateral membrane. Cell adhesion and motility assays demonstrated that *hepaCAM* increased cell spreading on the matrices fibronectin and matrigel, delayed cell detachment, and enhanced wound healing. Furthermore, when the cytoplasmic domain was deleted, *hepaCAM* mutants did not affect cell surface localization and dimer formation. Cell-matrix adhesion, however, was less significantly increased, and cell motility was almost unchanged when compared with the effect of the wild-type *hepaCAM*. Taken together, the cytoplasmic domain of *hepaCAM* is essential to its function on cell-matrix interaction and cell motility.

Cell adhesion is a dynamic process essential for the normal development and maintenance of tissues and organs in multicellular organisms. Cell-cell and cell-matrix interactions are mediated by a large and complex number of cell adhesion molecules expressed on the cell surface that interact with each other in a spatially and temporally regulated manner. According to their structural and functional features, cell adhesion molecules are generally classified into at least four major families: the cadherins, integrins, selectins, and members of the immunoglobulin superfamily (1–5). Apart from linking cells to

each other or to components of the extracellular matrix, an exciting concept that has emerged from recent cell biological research is that cell adhesion molecules function also as receptors critical in modulating signal transduction (6). Such interactions are vital for the regulation of cellular adhesion, proliferation, apoptosis, migration, and differentiation.

We have recently reported the identification of a novel gene in liver, designated as *hepaCAM* (GenBank™ AY047587), which was differentially expressed in human hepatocellular carcinoma. Located on human chromosome 11q24 and spanning 7 exons, *hepaCAM* encodes a novel member of the immunoglobulin superfamily. The predicted protein of 416 amino acids displays a typical structure of Ig-like adhesion molecules, including two extracellular Ig-like domains, a transmembrane segment, and a cytoplasmic tail. In addition, when exogenously expressed in the human hepatocellular carcinoma cell line HepG2, *hepaCAM* accelerates cell spreading and increases cell motility (7).

The mechanism of *hepaCAM* in mediating cell-matrix interaction is unknown. However, transfection studies with mutant and chimeric constructs of other adhesion molecules have suggested that the structural features of adhesion molecules play important roles in mediating their physiological and biological roles. Structure and function study of E-cadherin reveals that the formation of *cis*-dimer is fundamental for cell adhesion, and inhibition of *cis*-dimer formation is correlated with the lack of cell-cell interaction (8). For *HEPACAM1*, it has been proposed that both the first extracellular Ig domain and cytoplasmic domain are required for its adhesion function (9). Thus, defining the molecular organization of *hepaCAM* may help to elucidate the functional roles of *hepaCAM*.

In this study, we aimed to characterize the physiological and biological properties of *hepaCAM* and to investigate the importance of the cytoplasmic domain on *hepaCAM* functions in the *hepaCAM*-deficient MCF7 cells. We showed that *hepaCAM* is a phosphorylated glycoprotein that forms *cis*-homodimers on the cell surface and mediates cell-matrix interaction. In addition, the cytoplasmic domain is required for cell-matrix modulation but dispensable in subcellular localization and surface dimerization.

### EXPERIMENTAL PROCEDURES

**Plasmid Construction**—The complete coding sequence of *hepaCAM* and its mutants with truncated cytoplasmic domain were generated by PCR amplification. The cDNAs of *hepaCAM* residues 1–416 (wild-type), residues 1–320, or residues 1–269 were cloned into pEGFP-N2 vector (Clontech, Palo Alto, CA) or pcDNA3/V5-His vector (Invitrogen), at the HindIII/BamHI restriction sites. For polyclonal antibody generation, *hepaCAM* (residues 260–416) was cloned into the BglII/Sall restriction sites of the pQE40 vector (Qiagen). The sequences of the recombinant plasmids were verified by sequencing.

**Cell Culture and Transfection**—The MCF7 breast carcinoma cell line obtained from American Type Culture Collection (Manassas, VA) was maintained in the recommended conditions. Transfections of MCF7

\* This study was supported by the Biomedical Research Council of Singapore (Project No. 01/121/19/162). The costs of publication of this article were defrayed in part by the payment of page charges. This article must therefore be hereby marked "advertisement" in accordance with 18 U.S.C. Section 1734 solely to indicate this fact.

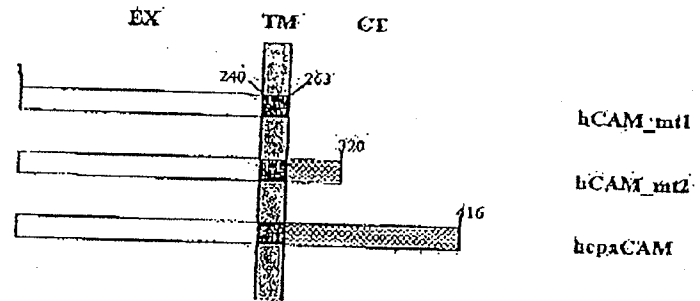
¶ To whom correspondence should be addressed: Dept. of Physiology, Faculty of Medicine, National University of Singapore, 2 Medical Dr., Singapore 117597, Republic of Singapore. Tel.: 65 68746406; Fax: 65-67788161; E-mail: phsssl@nus.edu.sg.

## Structure and Function of hepaCAM

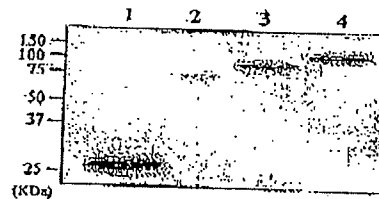
27867

A

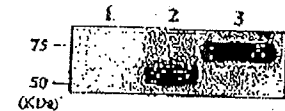
Fig. 1. Schematic representation and expression of wild-type and cytoplasmic domain mutants of hepaCAM. A, the wild-type and cytoplasmic domain mutants of hepaCAM were cloned into the eukaryotic expression vectors pEGFP-N2 and pCDNA3/V5-His and transfected into the breast carcinoma cell line MCF7. EX, extracellular domain (white box); TM, transmembrane domain (gray box); CT, cytoplasmic domain (dotted box). B, protein expression of pEGFPN2 vector and GFP-fused wild-type and mutant hepaCAM in MCF7 cells was detected by Western blotting using anti-GFP antibody. Lane 1, MCF7/pEGFPN2; lane 2, MCF7/hepaCAM\_mt1-GFP; lane 3, MCF7/hepaCAM\_mt2-GFP; lane 4, MCF7/hepaCAM-GFP. C, protein expression of pCDNA3/V5-His vector and V5-fused wild-type and mutant hepaCAM in MCF7 cells was detected by Western blotting using anti-V5 antibody. Lane 1, MCF7/pCDNA3; lane 2, MCF7/hepaCAM\_mt1-V5; lane 3, MCF7/hepaCAM-V5. Positions of the molecular size markers are shown on the left of each panel.



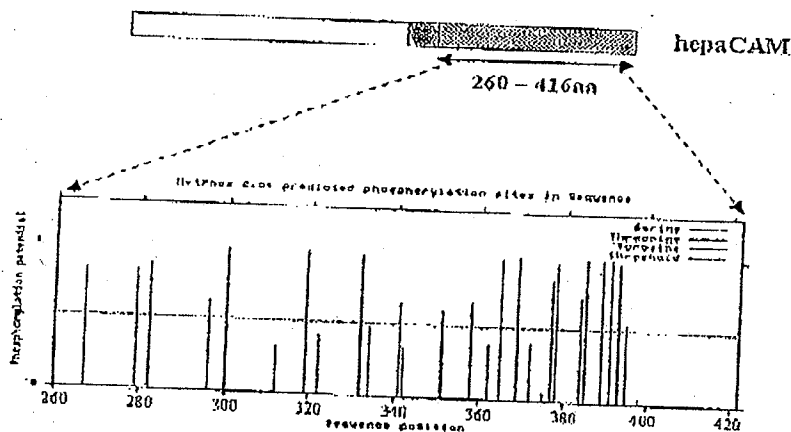
B



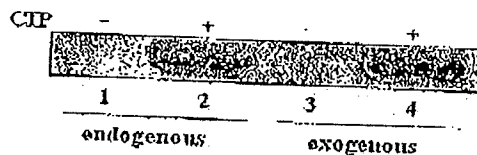
C



A



B



cells were carried out using the reagent Lipofectamine Plus (Invitrogen) according to the manufacturer's instructions. Transfected cells were selected for 4 weeks, either in the presence of 600  $\mu$ g/ml G418 or 10  $\mu$ g/ml blasticidin, and cloned.

**Western Blot Analysis.** Cells were lysed in radioimmunoprecipitation assay buffer to extract the total cell lysate. Immunoprecipitation was carried out by incubating the precleared cell lysate with the appropriate

mouse monoclonal antibody and horseradish peroxidase-conjugated protein G (Zymed Laboratories Inc., San Francisco, CA) overnight at 4 °C. Protein was resolved by SDS-PAGE, transferred onto membrane, and detected by either rabbit anti-hepaCAM polyclonal antiserum, mouse anti-V5 antibody (Invitrogen), mouse anti-GFP antibody (Santa Cruz Biotechnology, Santa Cruz, CA), or mouse anti-E-cadherin (Zymed Laboratories Inc.).

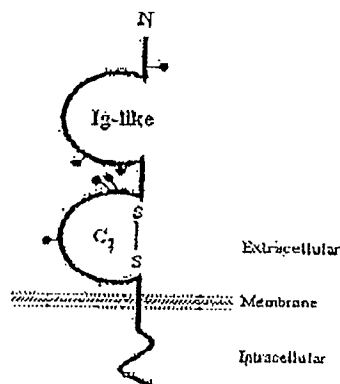
**Alkaline Phosphatase Treatment.** Cell lysate was incubated in de-

Fig. 2. Phosphorylation of hepaCAM cytoplasmic domain. A, residues 260-416 of hepaCAM was used to generate rabbit polyclonal antibody. Potential serine/threonine and tyrosine kinase phosphorylation sites in the cytoplasmic region were identified using NetPhos version 2.0 software. B, cell lysate prepared from C3A cells expressing endogenous hepaCAM (lanes 1 and 2) or MCF7/hepaCAM-V5 cells expressing exogenous hepaCAM (lanes 3 and 4) was either untreated (-) or treated (+) with calf intestinal alkaline phosphatase (CIP), as described under "Experimental Procedures." After dephosphorylation, hepaCAM protein was detected by Western blotting using the rabbit anti-hepaCAM polyclonal antiserum.

27368

## Structure and Function of hepaCAM

A



B

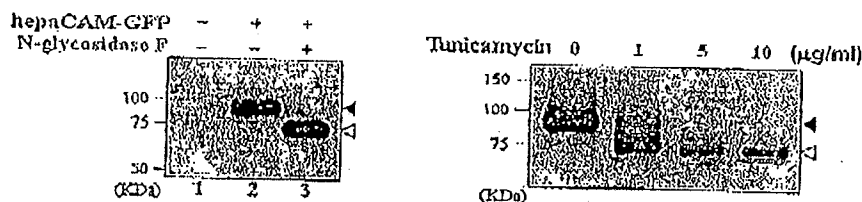


**FIG. 3. N-linked glycosylation of hepaCAM-GFP.** A, illustration of the secondary structure of hepaCAM protein. hepaCAM owns the typical structure of proteins in the immunoglobulin superfamily, including an extracellular segment consisting of an NH<sub>2</sub>-terminal-proximal Ig-like domain and a membrane-proximal C<sub>2</sub>-type Ig domain with a disulfide bond formed between two cysteine residues (S-S), a transmembrane region, and a cytoplasmic tail. The six putative N-linked glycosylation sites are indicated by the symbol "S". B, left panel, cell lysate was prepared from MCF7/hepaCAM-GFP (lanes 2 and 3) treated without (-) or with (+) N-glycosidase F. Untreated parental MCF7 cells (lane 1) were included as the control. Right panel, MCF7 cells transfected with hepaCAM-GFP were treated with tunicamycin at the indicated concentrations for 24 h before lysis. Protein samples were resolved by SDS PAGE and subjected to Western blotting with anti-GFP antibody. Solid and open arrowheads indicate signals for glycosylated and deglycosylated proteins, respectively. Positions of the molecular size markers are shown on the left.

phosphorylation buffer for 10 min at 30 °C. Calf intestinal alkaline phosphatase (Roche Applied Science) was added and incubated for a further 15 min prior to Western analysis.

**N-linked Glycosylation Analysis.** For inhibiting N-linked glycosylation, MCF7 cells were transiently transfected with hepaCAM-GFP and subsequently exposed to tunicamycin (Sigma) at the indicated concentrations for 24 h before lysis. For enzymatic digestion of N-linked oligosaccharides, the cell lysate of MCF7/hepaCAM-V5 was treated with peptide N-glycosidase F (New England Biolabs) according to the manufacturer's instructions. The samples were then subjected to Western analysis.

**Chemical Cross-linking.** A monolayer or a single suspension of cells was incubated in phosphate-buffered saline containing 3 mM BS<sup>3</sup> (Pierce) or DTSSP (Pierce) at room temperature for 30 min. The reaction was quenched with the addition of 20 mM Tris-HCl, pH 7.5, for 15 min. Single cell suspension was assured by microscopic observation before and after chemical cross-linking reaction. DTSSP-cross-linked proteins were resuspended in Laemmli sample buffer without 50 mM dithiothreitol, unless indicated. Cell lysate was prepared in radioimmunoprecipitation assay buffer containing 10 mM iodoacetamide (10).

**Immunocytochemistry.** Cells cultured on coverslips were fixed with 2% paraformaldehyde and permeabilized with 0.2% Triton X-100. Non-specific sites were blocked in 10% normal goat serum (Santa Cruz Biotechnology). Protein expression of V5-tagged hepaCAM was detected using mouse anti-V5 antibody, biotin-conjugated goat anti-mouse IgG antibody, and subsequently streptavidin-fluorescein. For co-localization experiments, cells were grown to confluence on 0.4-μm Transwell filters (Costar, Cambridge, MA). Protein expression of E-cadherin was detected using mouse anti-E-cadherin antibody, biotin-conjugated goat anti-mouse IgG antibody, and subsequently avidin-TRITC conjugate (Sigma). Fluorescence was visualized by fluorescence microscope (Carl Zeiss) or confocal microscope LSM 510 (Carl Zeiss) with sectioning performed at 0.5 μm.

**Cell Spreading.** Cells were seeded onto coverslips coated with 40 μg of matrigel basement membrane matrix (Colltech) or 10 μg/ml fibronectin (Santa Cruz Biotechnology) and incubated under standard culture conditions. Cell morphology was observed by microscopy. Unspread cells were defined as round cells, whereas spread cells were defined as cells with extended processes (11). The percentage of cells

demonstrating spread morphology was quantified in 10 randomly selected fields.

**Cell Detachment.** A confluent monolayer of cells was detached in 1 mM EDTA in phosphate-buffered saline at 37 °C. Cell detachment was evaluated under the inverted microscope at 5 and 15 min of incubation. Concurrently, the dissociated cells were harvested and counted in 10 randomly selected fields.

**Wound-healing Assay.** A confluent monolayer of cells was wounded with a sterile plastic 200-μl micropipette tip. The wound was observed microscopically at 24 and 48 h. The percentage of wound filling was calculated by measuring the remaining gap space on the pictures.

**Bioinformatics and Statistical Analysis.** The protein sequence of hepaCAM was analyzed using the NetPhos version 2.0 and Prosite programs. Nonparametric analysis of variance was performed to compare the difference among more than two means. Software InStat version 3.0 (GraphPad) was employed, and  $p < 0.01$  was considered significant.

## RESULTS

**Wild-type and COOH-terminal Mutants of hepaCAM.** The wild-type hepaCAM encodes a transmembrane Ig-like adhesion molecule of 416 amino acids. To assess the importance of hepaCAM cytoplasmic domain in its physiological and biological functions, we constructed two deletion mutants of hepaCAM. hCAM\_mt1, lacking the entire cytoplasmic tail, was constructed by truncating residues 284–416 of hepaCAM. hCAM\_mt2 was constructed by deleting residues 321–416 of hepaCAM to obtain a partial cleavage of the cytoplasmic tail (Fig. 1A). Wild-type hepaCAM, hCAM\_mt1, and hCAM\_mt2 were fused in-frame at the NH<sub>2</sub>-terminal of the green fluorescent protein (GFP) gene of the expression vector pEGFP-N2, and the resulting plasmids were named hepaCAM GFP, hCAM\_mt1-GFP, and hCAM\_mt2-GFP, respectively. In addition, wild-type hepaCAM and hCAM\_mt1 were inserted at the NH<sub>2</sub>-terminal of the V5 tag of the pcDNA6/V5-His vector and designated hepaCAM-V5 and hCAM\_mt1-V5, respectively. The constructs, as well as the empty vectors, were transfected into MCF7 cells, and the expressed proteins were analyzed by Western blotting using anti-GFP and anti-V5 antibodies accordingly (Fig. 1, B and C). Subsequently, MCF7 cells stably expressing pEGFP-N2 vector (MCF7/pEGFPN2), hepaCAM-GFP (MCF7/

<sup>1</sup> The abbreviations used are: BS<sup>3</sup>, bis(sulfosuccinimidyl) suberate; DTSSP, 3,3'-dithiobis (sulphosuccinimidyl propionate); GFP, green fluorescent protein; TRITC, tetramethylrhodamine isothiocyanate.

## Structure and Function of hepaCAM

27369

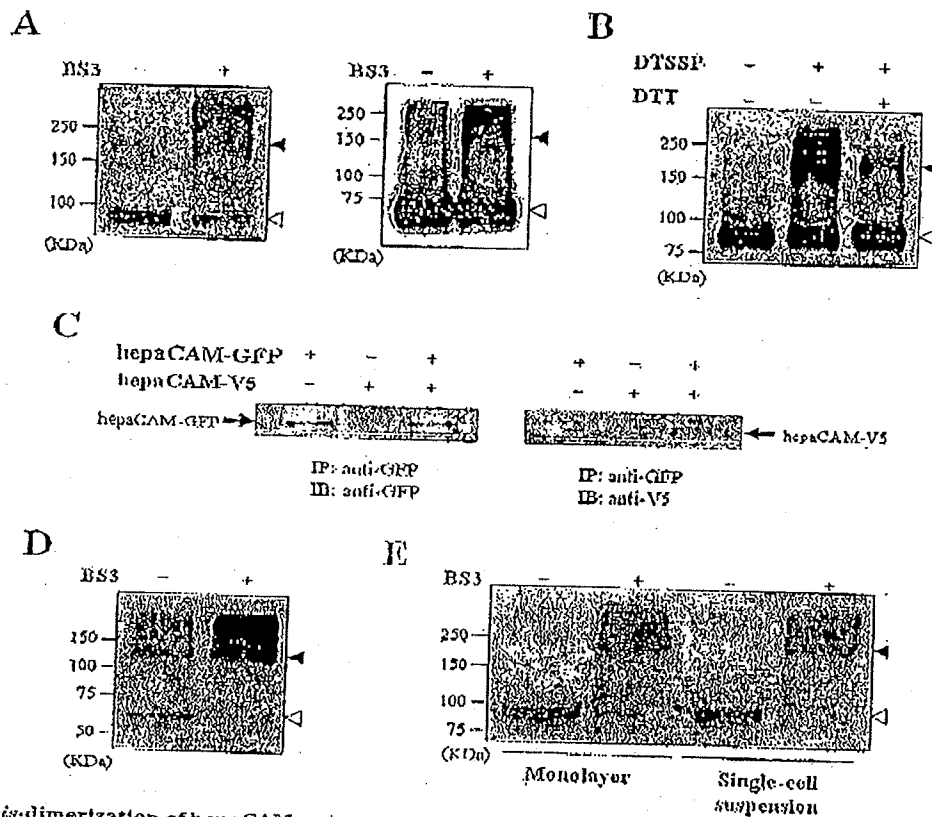


**FIG. 4. Homophilic cis-dimerization of hepaCAM and mutant.** A, cross-linking of hepaCAM-GFP (left panel) and hepaCAM-V5 (right panel) on the cell surface. A monolayer of MCF7/hepaCAM-GFP or MCF7/hepaCAM-V5 cells was untreated (–) and treated (+) with 3 mM BS3 prior to protein sample preparation in lysis buffer containing 10 mM iodoacetamide. Protein samples were subjected to Western blotting with anti-GFP antibody or anti-V5 antibody, respectively. B, a monolayer of MCF7/hepaCAM-GFP was untreated (–) and treated (+) with 3 mM DTSSP prior to protein sample preparation in lysis buffer containing 10 mM iodoacetamide. Protein samples were resuspended in Laemmli sample buffer in the presence (+) or absence (–) of dithiothreitol. C, co-immunoprecipitation of hepaCAM-GFP and hepaCAM-V5. MCF7 cells were transfected with hepaCAM-GFP, hepaCAM-V5, or both. Protein samples were prepared, immunoprecipitated with anti-GFP antibody, and subjected to Western blotting using anti-GFP antibody (left panel) or anti-V5 antibody (right panel). The signals corresponding to hepaCAM-GFP and hepaCAM-V5 molecules are marked with arrows. D, a monolayer of MCF7/hepaCAM-GFP cells was untreated (–) and treated (+) with 3 mM BS3 prior to protein sample preparation in lysis buffer containing 10 mM iodoacetamide. Protein samples were subjected to Western blotting with anti-GFP antibody. E, a monolayer and a single cell suspension of MCF7/hepaCAM-GFP were incubated in the absence (–) or presence (+) of 3 mM BS3. Protein samples were subjected to Western blotting with anti-GFP antibody. Solid and open arrowheads indicate signals for dimeric and monomeric proteins, respectively. \*, dimer in un-cross-linked sample. The positions of the molecular size markers are shown on the left of each panel.

hepaCAM-GFP, hCAM<sub>mt1</sub>-GFP (MCF7/hCAM<sub>mt1</sub>-GFP), hCAM<sub>mt2</sub>-GFP (MCF7/hCAM<sub>mt2</sub>-GFP), pcDNA6 vector (MCF7/pcDNA6), hepaCAM-V5 (MCF7/hepaCAM-V5) and hCAM<sub>mt1</sub>-V5 (MCF7/hCAM<sub>mt1</sub>-V5) were generated and cloned.

**Phosphorylation of the hepaCAM Cytoplasmic Domain**—We generated a polyclonal antiserum that recognizes the hepaCAM cytoplasmic domain but in its dephosphorylated form. The recombinant His bacterial fusion protein used for immunization contained residues 260–416 of hepaCAM. Western analysis showed that the resulting antiserum could specifically detect the bacterial fusion protein, otherwise undetectable by the pre-immune serum. However, when the antiserum was tested on the cell lysate of MCF7/hepaCAM-V5, no specific band was observed (data not shown). We suspected that the antiserum was unable to recognize the cytoplasmic domain of hepaCAM because of the presence of post-translational modifications, e.g. phosphorylation. Evaluation of the region selected for antibody generation by the NetPhos version 2.0 server predicted 28 potential serine-, threonine-, or tyrosine-phosphorylated residues scattered along the cytoplasmic do-

main of hepaCAM protein, with 20 of them giving a potential phosphorylation >0.5 (Fig. 2A). To verify that the hepaCAM cytoplasmic domain is phosphorylated, we dephosphorylated cell lysates of C3A cells expressing endogenous hepaCAM and MCF7/hepaCAM-V5 cells expressing exogenous hepaCAM with calf intestinal alkaline phosphatase. The untreated cell lysates were included as controls. Indeed, calf intestinal alkaline phosphatase-treated endogenous and exogenous hepaCAM were detected by the rabbit antiserum (Fig. 2B), confirming that the cytoplasmic domain of hepaCAM is phosphorylated.

**N-Linked Glycosylation of hepaCAM**—Sequence analysis of hepaCAM predicted six N-linked glycosylation sites on its extracellular domain (Fig. 3A). To investigate whether hepaCAM was glycosylated, the MCF7/hepaCAM-GFP cell lysate was enzymatically digested with peptide N-glycosidase F to release putative N-linked oligosaccharides. An untreated sample was included as the control. The molecular mass of hepaCAM-GFP, shown by Western analysis to be ~100 kDa, was shifted to ~75 kDa after deglycosylation. Consistently, when MCF7 cells transfected with hepaCAM-GFP were treated with tunicamycin (an antibiotic that inhibits N-linked glycosylation) at dif-

27370

## Structure and Function of hepaCAM

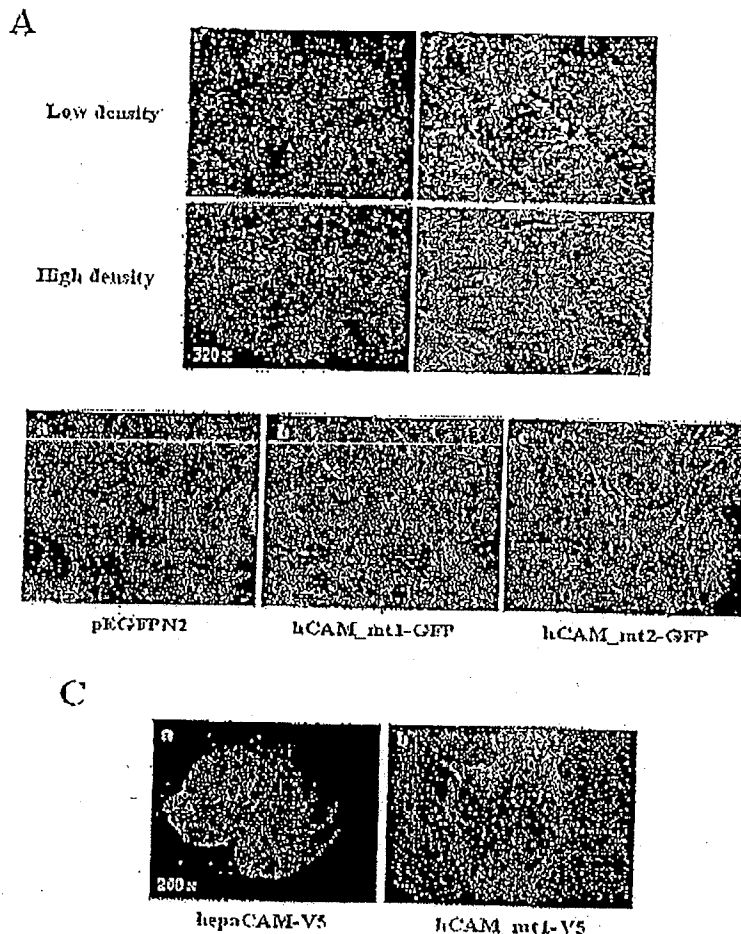


**Fig. 5. Subcellular localization of hepaCAM and mutants in MCF7 cells.** A, the localization of hepaCAM-GFP in MCF7 cells is cell density-dependent. MCF7/hepaCAM-GFP cells were seeded at low density and cultured for a few days. Cells at areas of low density (top panels) and high density (bottom panels) were observed under a fluorescence (left panels) or inverted microscope (right panels). Magnification is  $\times 320$ . B, the expression of pEGFP-N2 (a), hCAM\_mtl1-GFP (b), and hCAM\_mtl2-GFP (c) in MCF7 cells was detected by fluorescence microscopy. Magnification is  $\times 340$ . C, MCF7/hepaCAM-V5 (a) and MCF7/hCAM\_mtl1-V5 (b) cells were immunostained with anti-V5 antibody to detect localization of hepaCAM and mutant under a fluorescence microscope. Magnification is  $\times 200$ .

ferent doses for 24 h, a band at  $\sim 75$  kDa was also observed (Fig. 3B). The results verified that hepaCAM is a glycoprotein. By subtracting the molecular mass of GFP, i.e. 27 kDa, the deglycosylated form of hepaCAM is  $\sim 48$  kDa.

**Dimerization of hepaCAM and Mutant on Plasma Membrane.**—We evaluated the pre-existing forms of hepaCAM on cell membrane by incubating a monolayer of MCF7/hepaCAM-GFP cells with BS3, a noncleavable membrane-impermeable cross-linker. The cell lysate was prepared in the presence of iodoacetamide to inhibit the formation of nonspecific disulfide bonds (10). An untreated sample was included as the control. The samples were analyzed by Western blotting with anti-GFP. In the presence of BS3, a band of  $\sim 200$  kDa appeared, which seemed to represent the dimerized form of hepaCAM-GFP, accompanied with the disappearance of the hepaCAM monomers. Similarly, treatment of MCF7/hepaCAM-V5 cells with BS3 resulted in a decrease of the  $\sim 75$ -kDa monomeric form of hepaCAM and an accumulation of the higher molecular weight species at  $\sim 150$  kDa, although no distinct band was noted (Fig. 4A). It is possible that the anti-V5 antibody did not recognize the higher molecular weight species as efficiently as monomers. To examine whether hepaCAM forms a homodimer on the cell surface, MCF7/hepaCAM-GFP cells were treated with DTSSP, a reducible membrane-impermeable cross-linker. In the absence of the reducing agent dithiothreitol, a significant increase in the 200-kDa species was observed. However, when dithiothreitol was added into the sample buffer, the higher molecular mass was reduced to the monomeric form to a level

closely comparable with that of the untreated cells (Fig. 4B). Additionally, we co-expressed hepaCAM-GFP and hepaCAM-V5 in MCF7 cells, immunoprecipitated the cell lysate with anti-GFP antibody, and immunoblotted with anti-V5 or anti-GFP. The result revealed co-immunoprecipitation of hepaCAM-GFP with hepaCAM-V5 (Fig. 4C), demonstrating that hepaCAM molecules dimerized through homophilic interaction. To examine whether tailless hepaCAM proteins form dimers, MCF7/hCAM\_mtl1-GFP cells were treated with BS3 and analyzed by Western blotting (Fig. 4D). The monomeric form of hCAM\_mtl1-GFP was diminished and replaced with its dimeric form at  $\sim 125$  kDa in the BS3-treated sample. Interestingly, in the untreated sample of hepaCAM-GFP and hCAM\_mtl1-GFP, protein species that seemed to represent the dimeric form of the proteins were observed. This phenomenon could be due to covalent bonding between the dimers of hepaCAM-GFP or hCAM\_mtl1-GFP. To determine whether hepaCAM-GFP forms *cis*- or *trans*-dimers on the cell surface, both adherent monolayer and single cell suspension of MCF7/hepaCAM-GFP cells were treated with BS3 (Fig. 4E). The extent of dimerization was comparable in both adherent and suspension cells, indicating that hepaCAM homodimerization occurs predominantly through *cis*-interactions rather than *trans*-interactions within the plane of the membrane of individual cells.

**Subcellular Localization of hepaCAM and Mutants in MCF7 Cells.**—We explored the subcellular distribution of wild-type hepaCAM in MCF7/hepaCAM-GFP cells at low and at high cell densities by fluorescence and inverted microscopy (Fig. 5A). When

## Structure and Function of hepaCAM

27371

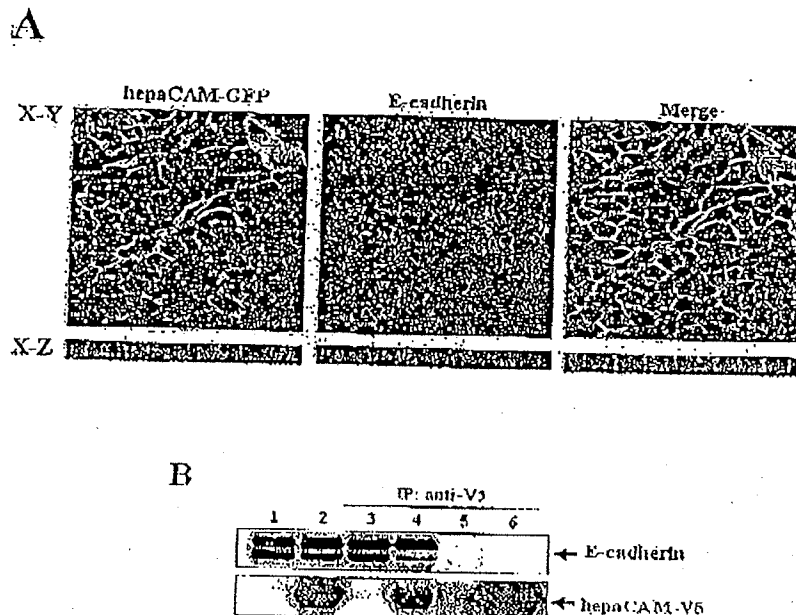


**FIG. 6. Co-localization of hepaCAM with E-cadherin.** *A*, MCF7/hepaCAM-GFP cells grown to confluence on the Transwell filter unit were fixed, permeabilized, and immunostained with anti-E-cadherin. Laser scanning confocal microscopy was performed with a filter set suitable for fluorescein and rhodamine detection. The representative sets of X-Y and X-Z sections are indicated. *a*, hepaCAM-GFP stained green; *b*, E-cadherin stained red; *c*, confocal images of the hepaCAM GFP and E-cadherin were merged to show regions of co-localization. *D*, co-immunoprecipitation of (IP) with anti-V5 antibody and subjected to Western blotting using anti-E-cadherin (top panel) or anti V5 antibody (bottom panel). The signals lysate of MCF7/hepaCAM-V5 before IP; lane 3, cell lysate of MCF7/pcDNA6 after IP; lane 4, cell lysate of MCF7/hepaCAM-V5 after IP; lane 5, precipitate of MCF7/pcDNA6; lane 6, precipitate of MCF7/hepaCAM-V5.

cells were well spread, hepaCAM protein was localized to punctuate structures in the perinuclear membrane, cytoplasm, and at the tip of the cell surface protrusions, which were about to make contact with adjacent cell surfaces, forming zipper-like structures. Once the cells became confluent, the protein was localized at a lesser extent in the perinuclear membrane and cytoplasm and predominantly on the plasma membrane, particularly in the areas of cell-cell contacts. The results suggest that the sub-cellular localization of hepaCAM is cell density-dependent. We also examined the effect of hepaCAM cytoplasmic domain in its plasma membrane localization. hCAM\_mt1-GFP and hCAM\_mt2-GFP were both recruited to the plasma membrane of MCF7 cells (Fig. 5B). Similarly, MCF7/hepaCAM-V5 and MCF7/hCAM\_mt1-V5 cells immunostained with anti-V5 showed that hepaCAM and its mutant were predominantly expressed on cell membranes (Fig. 5C). The results indicate that the cytoplasmic domain is dispensable for membrane localization.

**Co-localization of hepaCAM with E-cadherin**—The distribution of hepaCAM was further examined in confluent polarized MCF7/hepaCAM-GFP cells by confocal laser scanning microscopy (Fig. 6A). The cells were also stained for E-cadherin, which localizes in the lateral cell surface, to compare its localization with that of hepaCAM. In the X-Y sections, hepaCAM-GFP was distributed to honeycomb-like structures at cell-cell boundaries, which significantly co-localized with E-cadherin. In the X-Z vertical cross-section, the distribution of E-cadherin along the entire lateral cell surface coincided with hepaCAM-GFP. Moreover, hepaCAM was detected at the basal membrane that was in contact with the Transwell membrane. Because hepaCAM and E-cadherin appeared to co-localize, we investigated whether there were any physical interactions between them by co-immunoprecipitation (Fig. 6B). Cell lysate prepared from MCF7/hepaCAM-V5 was precipitated with the anti-V5

antibody and subjected to Western blotting using the anti-E-cadherin or anti-V5 antibodies. MCF7/pcDNA6 cell lysate was included in the experiment as the control. No co-immunoprecipitation was observed, suggesting that E-cadherin and hepaCAM do not physically interact.

**Cell-Matrix Interaction by hepaCAM and Mutant**—We evaluated the adhesive properties of V5-tagged hepaCAM and mutant constructs on the MCF7 cells through cell aggregation, cell adhesion, and detachment assays. No clear change in cell aggregation was observed among MCF7/pcDNA6, MCF7/hCAM\_mt1-V5, and MCF7/hepaCAM-V5 cells (data not shown), but hepaCAM was capable of modulating cell-matrix adhesion significantly. Fig. 7 shows that ~60 and 79% of the MCF7/hepaCAM-V5 cells exhibited spread morphology on fibronectin at 30 min and 2 h of incubation, respectively, in contrast to 40.8 and 58.2% of the MCF7/hCAM\_mt1-V5 cells and 7.8 and 18% of MCF7/pcDNA6 cells ( $p < 0.001$ ). Similarly on matrigel, MCF7/hepaCAM-V5 cells showed the fastest spreading, followed by MCF7/hCAM\_mt1-V5 cells, and then MCF7/pcDNA6 cells ( $p < 0.001$ ). In the cell detachment assay (Fig. 8), MCF7/hepaCAM-V5 cells detached 18.9 and 21.6 times slower than MCF7/pcDNA6 cells at 5 and 15 min, respectively. MCF7/hCAM\_mt1-V5 cells, on the other hand, detached ~4 and 2.2 times slower than MCF7/pcDNA6 cells at time points 5 min and 15 min ( $p < 0.001$ ). The results showed that, in addition to its extracellular and transmembrane domains, hepaCAM needs its cytoplasmic domain to mediate strong cell-matrix adhesion.

**Cell Motility by hepaCAM and Mutant**—Cell motility of hepaCAM and mutant was assessed by matrigel invasion and wound-healing assays. Barely any MCF7 cells expressing pcDNA6, hCAM\_mt1, and hepaCAM migrated through the 8- $\mu$ m Transwell membrane (data not shown). This observation could be explained by the poorly invasive nature of MCF7 cells.

27372

## Structure and Function of hepaCAM

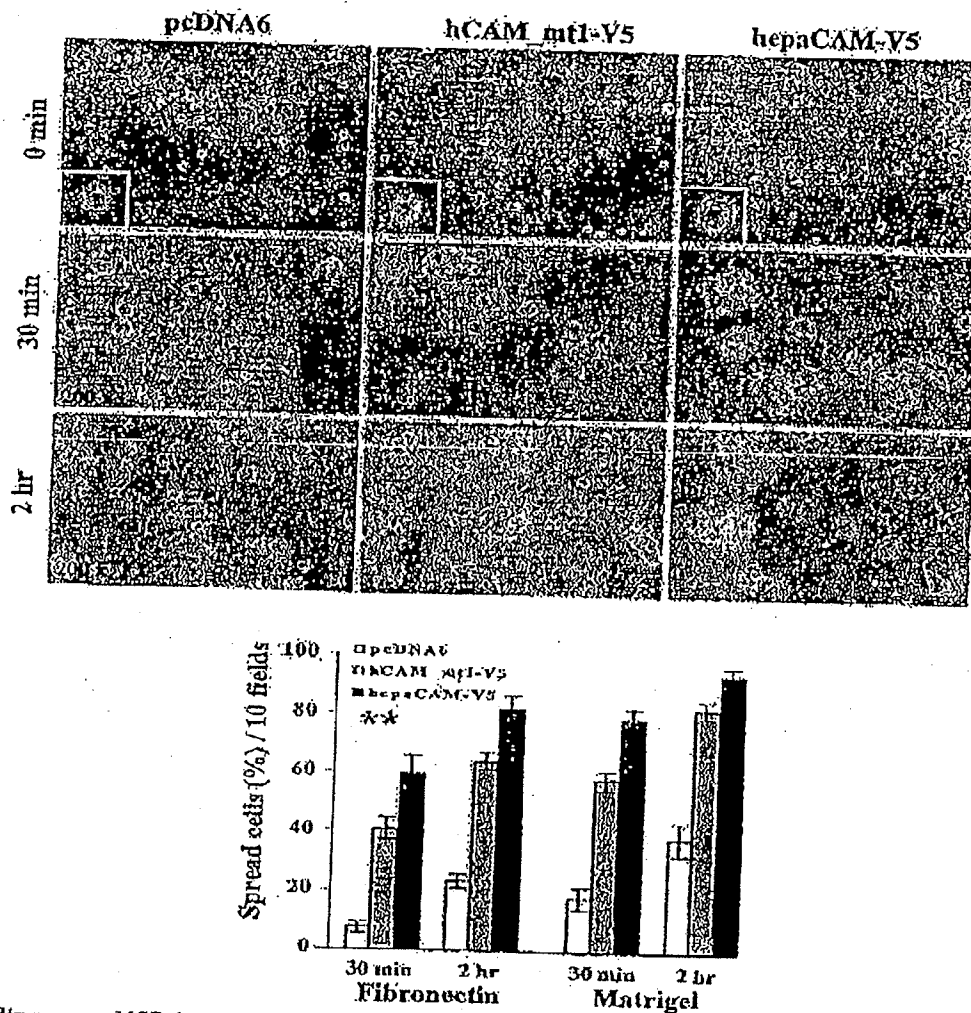


FIG. 7. Cell spreading assay. MCF7/pcDNA6 (left panels), MCF7/hCAM\_mt1-V5 (middle panels) and MCF7/hepaCAM-V5 (right panels) cells were allowed to spread on matrigel-coated coverslips for 30 min or 2 h. Insets, cell morphology before spreading. The microscopic photos were taken under  $\times 200$  magnification. Shown is the percentage of spread cells on fibronectin and matrigel. At 30 min or 2 h after plating, the total number of cells showing spread morphology were counted in ten randomly selected fields, and the percentage of cell spreading was then computed. The data represent means  $\pm$  S.D. ( $n = 6$ ); \*\*,  $p < 0.001$  as assessed by analysis of variance.

Moreover, MCF7/hepaCAM cells were enlarged, therefore retarding migration. However, in the wound-healing assay (Fig. 9), we demonstrated that, after 24 h of incubation, MCF7/hepaCAM-V5 cells filled 59.8% of the scratched area ( $p < 0.01$ ), compared with 36.3% by MCF7/hCAM\_mt1-V5 cells ( $p > 0.05$ ) and 38.1% by MCF7/pcDNA6 cells. After 48 h, MCF7/hepaCAM-V5 cells closed 83.7% of the wound ( $p < 0.01$ ), compared with 55.2% by MCF7/hCAM\_mt1-V5 cells ( $p > 0.05$ ) and 49.5% by MCF7/pcDNA6 cells. Hence, the cytoplasmic domain is important for cell motility modulated by hepaCAM.

## DISCUSSION

In our previous work, we identified a novel Ig-like molecule, hepaCAM, which exhibits typical structural characteristics of adhesion molecules of the immunoglobulin superfamily (7). In this study, we demonstrated physiological and biological characteristics of hepaCAM and the relationship between its structure and function, particularly with respect to the cytoplasmic domain.

Sequence analysis revealed that the cytoplasmic domain of hepaCAM contains a proline-rich region that provides putative

binding sites for SH3 domains and potential phosphorylation sites of serine/threonine and tyrosine kinases. Experimentally, we showed that the cytoplasmic domain is phosphorylated, suggesting an important role of the hepaCAM cytoplasmic domain in signaling cascades controlling cellular adhesion, motility, morphology, and all processes depending on the cytoskeleton. To evaluate the significance of the cytoplasmic domain, we transfected wild-type and cytoplasmic domain-truncated constructs of hepaCAM into MCF7 cells and analyzed their effects on hepaCAM functions.

Biochemical analysis revealed that hepaCAM is a glycosylated protein and forms a cis-homodimer on the cell surface. Deletion of the cytoplasmic domain did not interfere with dimer formation, suggesting that dimerization may be stabilized by the extracellular and/or transmembrane domains but not the cytoplasmic domain. Notably, chemical cross-linking of hepaCAM or its mutated protein both showed the presence of high molecular weight proteins, indicating that hepaCAM may form large complexes with other endogenously expressed cellular proteins through its extracellular and/or transmembrane do-



## Structure and Function of hepaCAM

27373

FIG. 8. Cell detachment assay. MCF7/pcDNA6 (left panels), MCF7/hCAM<sub>mt1-V5</sub> (middle panels), and MCF7/hepaCAM-V5 (right panels) cells were detached in 1 mM EDTA for 5 min or 15 min. The microscopic photos were taken under X200 and X400 magnifications. At 5 min or 15 min after incubation, the total number of detached cells was counted in ten randomly selected fields, and the percentage of cell detachment was then computed. The data represent means  $\pm$  S.D. ( $n = 6$ ), \*\*,  $p < 0.001$  as assessed by analysis of variance.

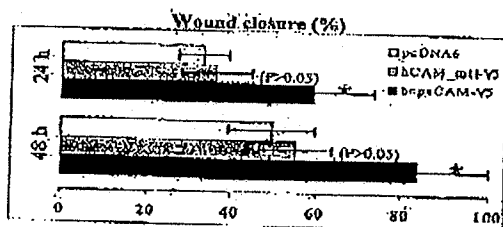
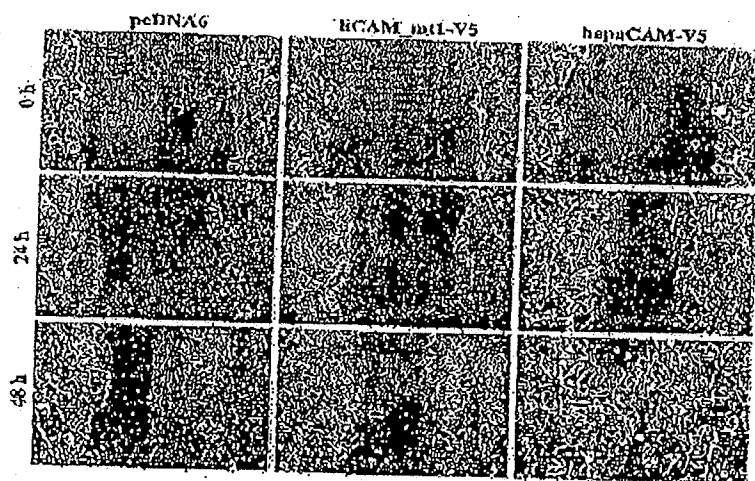
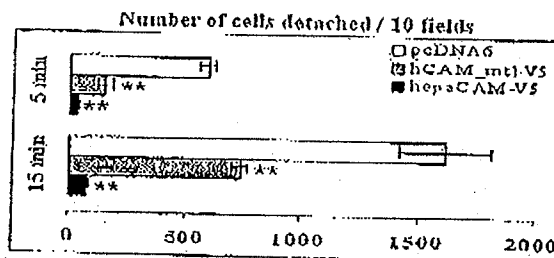
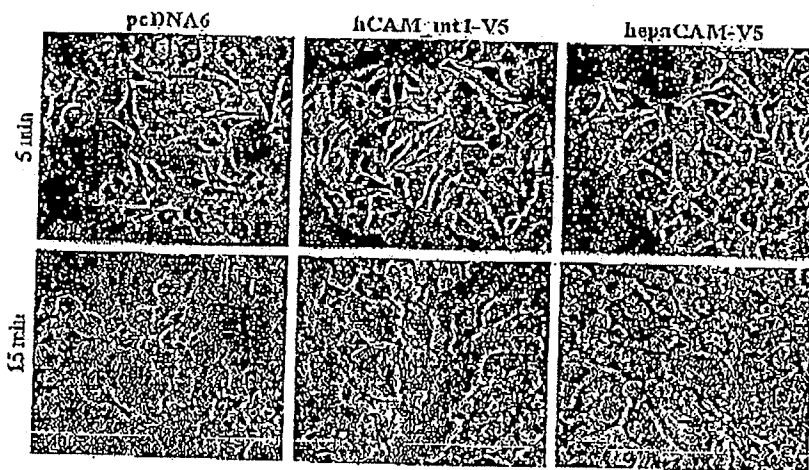


FIG. 9. Wound-healing assay. Wounds were made by pipette tip on confluent MCF7/pcDNA6 (left panels), MCF7/hCAM<sub>mt1-V5</sub> (middle panels), and MCF7/hepaCAM-V5 (right panels) cells and allowed to heal for 24 and 48 h. The microscopic photos were taken under X100 magnification. The diameters of wounds were measured on the microscopic photos at 0, 24, and 48 h after wounding. Changes in wound diameter were computed into percentage (means  $\pm$  S.D.,  $n = 6$ ) to represent wound closure. \*,  $p < 0.01$  as assessed by analysis of variance.

mains. Alternatively, it may represent higher order homo-oligomers of hepaCAM or its mutant. It is interesting to observe the seemingly dimeric form of hepaCAM and its mutant in their respective un-cross-linked samples. Although the mechanism resulting in such interaction is unknown to us, Hunter et

al. (5) and others (12) have observed a similar phenomenon in C-CAM and raise the possibility that C-CAM dimers become covalently linked, perhaps through the action of transglutaminase, an enzyme which catalyzes the formation of  $\gamma$ -glutamyl-lysine bonds in a restricted number of cellular proteins.



## Structure and Function of hepaCAM

Subcellular localization of hepaCAM in nonpolarized MCF7 cells showed that hepaCAM molecules were recruited to the cytoplasmic membranes at sites of cell-cell attachment. In polarized cells, hepaCAM was preferentially expressed in the lateral and basal membranes. Co-localization analysis demonstrated that hepaCAM co-localized laterally with E-cadherin, but no physical interaction between the two molecules was detected. We also showed that partial truncation and complete deletion of the cytoplasmic domain did not alter the plasma membrane localization. It has been reported that the CEACAM1 cytoplasmic domain regulates its lateral localization. Differing in their cytoplasmic domains, isoform CEACAM1-S distribution is exclusively apical, whereas isoform CEACAM1-L occurs both in apical and lateral cell surfaces (13). However, whether the loss of cytoplasmic domain affects the lateral and basal localization of hepaCAM remains to be determined.

Functionally, hepaCAM is capable of modulating cell-matrix interaction. Cell adhesion to the substratum plays a crucial role in cell migration, which is a key aspect of many normal and abnormal biological processes, including embryonic development, immunity, wound healing, and metastasis of tumor cells (14, 15). The distribution of hepaCAM on the basal membrane of cells, in addition to the spread morphology of MCF7/hepaCAM-V5 cells, hinted at possible *trans*-interaction between hepaCAM and the substratum. Evidently, cell spreading, cell detachment, and wound-healing assays revealed increased cell-substrate affinity and cell motility mediated by hepaCAM. Deletion of the cytoplasmic domain reduced, but did not completely abrogate, cell-matrix adhesion mediated by the wild-type hepaCAM, implicating that, to a considerable extent, the extracellular and transmembrane domains are able to initiate adhesion. However, the rate of wound healing of cells expressing mutant hepaCAM was close to the level of the control cells, indicating that the cytoplasmic domain is essential for mediating wound recovery. The data implies that cell-matrix adhesion and cell motility are controlled separately, and phosphorylation of the cytoplasmic domain may play a pivotal role in the regulation. Indeed, phosphorylation of CD44 was shown to regulate melanoma cell and fibroblast migration on, but not attachment to, a hyaluronan substratum (16). Additionally, it has been proposed for the cadherins (8, 17, 18) and for CEA (19) that

*cis*-dimerization will lead to strengthened cell adhesion, and *cis*-homodimer formation of ICAM-1 enhances its binding to a leukocyte  $\beta 2$ -integrin (20). However, the functional significance of hepaCAM post-translational modification and dimerization in regulating cell-matrix interaction is still under investigation.

In conclusion, we have shown that hepaCAM is a phosphorylated glycoprotein, forms *cis*-homodimers on the cell surface, and modulates cell-matrix interaction. The cytoplasmic domain, although unessential for cell surface localization and dimerization, is required to maintain a complete functional form of hepaCAM as a modulator of cell-matrix interaction.

**Acknowledgment**—We thank Ashu Reka Das for her assistance whenever and wherever needed.

## REFERENCES

- Edelman, G. M. (1986) *Annu. Rev. Cell Biol.* 2, 81-116
- Edelman, G. M. (1984) *Proc. Natl. Acad. Sci. U. S. A.* 81, 1460-1464
- Edelman, G. M., and Crossin, K. L. (1991) *Annu. Rev. Biochem.* 60, 155-190
- Taketsuchi, M. (1991) *Science* 251, 1461-1465
- Hunter, I., Sawa, H., Edlund, M., and O'Brien, B. (1996) *Biochem. J.* 320, 847-853
- Rosales, C., O'Brien, V., Kornberg, L., and Juliano, R. (1996) *Biochim. Biophys. Acta* 1242, 77-98
- Moh, M. C., Lee, L. H., and Shen, S. (2005) *J. Hepatol.* 43, 838-841
- Takeda, H., Shimoyama, Y., Nagafuchi, A., and Hirohashi, S. (1999) *Nat. Struct. Biol.* 6, 310-312
- Cheung, P. H., Luo, W., Qiu, Y., Zhang, X., Barley, K., Millireux, P., and Liu, S. H. (1994) *J. Biol. Chem.* 269, 24303-24310
- Masuda, M., Yageta, M., Fukuhara, H., Kuramoto, M., Murayama, T., Nomoto, A., and Murakami, Y. (2002) *J. Biol. Chem.* 277, 31014-31019
- Richardson, A., Malik, R. K., Hildebrand, J. D., and Pasternak, J. T. (1997) *Mol. Cell. Biol.* 17, 6906-6914
- Greenberg, C. E., Birchbichler, P. J., and Rice, R. H. (1991) *FASEB J.* 5, 3071-3077
- Sundberg, U., Beauclercq, N., and O'Brien, B. (2004) *J. Cell Sci.* 117, 1091-1104
- Nedhar, S., and Hammigan, G. E. (1996) *Curr. Opin. Cell Biol.* 8, 657-669
- Xie, H., Pallero, M. A., Gupta, K., Chang, P., Ware, M. F., Witke, W., Kwiatkowski, D. J., Lauffenburger, D. A., Murphy-Ullrich, J. E., and Wells, A. (1998) *J. Cell Sci.* 111, 615-624
- Peck, D., and Isacku, C. M. (1996) *Curr. Biol.* 6, 884-890
- Shapiro, I., Fannon, A. M., Kwong, P. H., Thompson, A., Lehmann, M. S., Grubel, G., Lagrand, J. P., Aiz-Nielsen, J., Culman, D. K., and Hendrickson, W. A. (1995) *Nature* 374, 327-337
- Nagar, B., Oveidun, M., Ikura, M., and Rini, J. M. (1996) *Nature* 380, 360-364
- Bates, P. A., Luo, J., and Sternberg, M. J. (1992) *FEBS Lett.* 301, 207-214
- Reilly, P. L., Woska, J. R., Jr., Jemal, D., McNally, E., Rodin, R., and Dormann, B. J. (1996) *J. Immunol.* 156, 528-532

EPO-231

04.09.2008

GLIA 56:633-646 (2008)



# GlialCAM, an Immunoglobulin-Like Cell Adhesion Molecule is Expressed in Glial Cells of the Central Nervous System

LINDA FAVRE-KONTULA,<sup>1</sup> ALEXANDRE ROLLAND,<sup>2</sup> LILIA BERNASCONI,<sup>3</sup> MARIA KAIMIRANTZOU,<sup>4</sup> CHRISTINE POWELL,<sup>1</sup> BRUNO ANTONSSON,<sup>1</sup> AND URSULA BOSCHERT<sup>1\*</sup>

<sup>1</sup>Protein and Cell Sciences, Merck Serono, Geneva Research Center, Geneva, Switzerland

<sup>2</sup>Immunology Department, Merck Serono, Geneva Research Center, Geneva, Switzerland

<sup>3</sup>Neurology Department, Merck Serono, Geneva Research Center, Geneva, Switzerland

<sup>4</sup>Bioinformatics Department, Merck Serono, Geneva Research Center, Geneva, Switzerland

## KEY WORDS

hepaCAM; ependymal cells; oligodendrocytes; astrocytes; myelination; GAP43

## ABSTRACT

Using structure based genome mining targeting vascular endothelial and platelet derived growth factor immunoglobulin (Ig) like folds, we have identified a sequence corresponding to a single transmembrane protein with two Ig domains, which we cloned from a human brain cDNA library. The cDNA is identical to hepatocyte cell adhesion molecule (hepaCAM), which was originally described as a tumor suppressor gene in liver. Here, we show that the protein is predominantly expressed in the mouse and human nervous system. In liver, the expression is very low in humans, and is not detected in mice. To identify the central nervous system (CNS) regions and cell types expressing the protein, we performed a LacZ reporter gene assay on heterozygous mice in which one copy of the gene encoding the novel protein had been replaced with  $\beta$ -galactosidase.  $\beta$ -galactosidase expression was prominent in white matter tracts of the CNS. Furthermore, expression was detected in ependymal cells of the brain ventricular zones and the central canal of the spinal cord. Double labeling experiments showed expression mainly in CNPase positive oligodendrocytes (OL). Since the protein is predominantly expressed in the CNS glial cells, we named the molecule glial cell adhesion molecule (GlialCAM). A potential role for GlialCAM in myelination was supported by its up-regulation during postnatal mouse brain development, where it was concomitantly expressed with myelin basic protein (MBP). In addition, *in vitro*, GlialCAM was observed in various developmental stages of OL and in astrocytes in processes and at cell contact sites. In A2B5 positive OL, GlialCAM colocalizes with GAP43 in OL growth cone like structures. Overall, the data presented here indicate a potential function for GlialCAM in glial cell biology. © 2008 Wiley-Liss, Inc.

involved in many other physiological processes such as cellular motility, migration, proliferation, and differentiation (Rafas and Ahmed, 1999). CAMs are generally classified into four major families according to their structure: the integrins, the selectins, the cadherins, and the immunoglobulin (Ig) superfamily of adhesion molecules (IgCAMs), which constitute the largest repertoire in vertebrates (Barclay, 2003).

IgCAMs are particularly abundant in the nervous system (NS) where they are implicated in diverse stages of brain development and are important for brain morphology as well as for many general NS functions (Sakisaka and Takai, 2005). During early NS development, IgCAMs such as neural cell adhesion molecule (NCAM) or I.1 are involved in neuronal migration, axon guidance, target recognition, and synapse formation. However, they also participate in the maintenance and function of neuronal networks in the adult (Dityatev et al., 2004; Maness and Schachner, 2007). The importance of IgCAMs in the central nervous system (CNS) has mainly been investigated in neurons but recent studies indicate that these proteins also play a role in migration, process guidance and target recognition in glial cells (Fox et al., 2006). Furthermore, several IgCAMs are involved in the formation and stability of the myelin sheath wrapping the axons through the interactions between axons and the myelinating cells of the central and peripheral NS, oligodendrocytes, and schwann cells, respectively. The envelopment of axons with myelin is essential for efficient nerve conduction, and thus for the proper functioning of the NS (Sherman and Brophy, 2005). Furthermore, various CAMs have been described to be important for the integrity of ependymal cells, which line the cavities of the CNS and make up the walls of the ventricles. These ciliated epithelial

## INTRODUCTION

Cellular adhesion molecules (CAMs) are cell surface receptors mediating cell-cell and cell-extracellular matrix interactions. They are not only essential for the maintenance of organs and tissue structures, but are

This article contains supplementary material available via the Internet at <http://www.interscience.wiley.com/jpages/0894-1491/suppmat>.

The authors contributed equally to this work.

\*Correspondence to: Ursula Boschert, Merck Serono International SA, 9, Chemin des Mines, 1204 Geneva, Switzerland. E-mail: boschert.ursula@merckserono.net

Received 12 September 2007; Accepted 21 December 2007

DOI 10.1002/glia.20640

Published online 21 February 2008 in Wiley InterScience (www.interscience.wiley.com).

## GLIALCAM EXPRESSION IN THE CNS

635

phate dehydrogenase (GAPDH), which was amplified using primers 5'-CCACCCATGGCAAATTC-3' and 5'-GATGGGATTTCATTGATGACA-3'. Mouse *GlialCAM* was amplified using primers 5'-GGGAGAAGAACATCAACCT-3' and 5'-TGAGCTCCAGCACAGTGGT-3' and its expression was quantified with the housekeeping gene  $\beta$ -actin and the following primers: 5'-AACCCCTAAGGCCAACCTGA-3' and 5'-GCCTGGATGGCTACGTACATG-3'. The expression levels of the target genes were normalized to the internal housekeeping genes and analyzed using the SDS 2.2.2 software system (Applied Biosystems).

## Western Blot Analysis

Human tissue lysates (Prosci Incorporated, Foway, CA) were supplied in SDS sample buffer containing 5%  $\beta$ -mercaptoethanol. Mouse tissue lysates were prepared as follows: specific organs from adult C57BL/6 mice were removed after intracardial PBS perfusion and homogenized in 50 mM Tris pH 8 containing 150 mM NaCl, 0.02%  $\text{NaN}_3$ , 0.1% SDS, 1% NP-40, 0.5% sodium deoxycholate, and an EDTA-free protease inhibitor cocktail (Roche, Basel, Switzerland) using a polytron. Large debris and unbroken cells were removed by centrifugation. The supernatant was collected and the protein concentration determined using a modified Bradford assay (Bio-Rad).

For WB analysis, 20  $\mu$ g of tissue extracts were separated on a NuPAGE<sup>®</sup> 4–12% Bis-Tris gradient gel (Invitrogen) and transferred onto a 0.2  $\mu$ m nitrocellulose membrane. Membranes were blocked with TBS containing 0.1% Tween-20 and 5% skimmed milk and incubated at 4°C overnight with primary antibody. After three washes, membranes were incubated with peroxidase-coupled secondary antibodies against rabbit and mouse IgG (Dako, Glostrup, Denmark). Bands were then visualized using an ECL detection system (GE Healthcare, Little Chalfont, United Kingdom). Mouse monoclonal anti-actin antibody (Chemicon, Temecula, CA) and anti-GAPDH antibody (Ambion, Austin, TX) were used as loading controls.

For the expression study during postnatal development, the total brain of C57BL/6 mice was dissected at various time-points and treated as above. To quantify *GlialCAM* expression, four mice were analyzed per time point and protein bands were quantified by densitometric scanning ( $\text{OD} \times \text{mm}^2$ ) using a GS-800 calibrated densitometer and related software (Bio-Rad). *GlialCAM* specific bands were then normalized to GAPDH band levels. To study the distribution of *GlialCAM* in mouse brain, we used an adult mouse brain blot containing 12 distinct brain areas of a Balb/c male (Chemicon). The blot was treated as described earlier.

Generation of *GlialCAM* Deficient Mice and *Lac-Z* Staining

*GlialCAM* deficient mice were generated using the Velocigene technology (Regeneron, Tarrytown, NY) as described previously (Valenzuela et al., 2003). Briefly, the

genomic sequence of *GlialCAM* was replaced by a cassette containing the coding sequence of  $\beta$ -galactosidase (*lac-Z*) and Lox flanked neomycin gene driven by a mammalian promoter (supplementary Fig. 1). For the *Lac-Z* reporter gene assay, in wild type and *GlialCAM* heterozygous mice, tissues were fixed by transcardial perfusion with PBS containing 4% paraformaldehyde. The tissues were removed, carefully dissected, frozen, and cut with a cryostat at a thickness varying from 10 to 40  $\mu$ m. To measure  $\beta$ -galactosidase activity, sections were incubated with substrate solution for 12 h. The reaction was then stopped and tissue sections were counterstained with nuclear red.

To identify the cell types expressing *GlialCAM* *in vivo*, we performed double immunohistochemical staining on heterozygous tissue sections. Sections were incubated overnight at 4°C with the following primary antibodies (dilution 1:100 to 1:2,000): rabbit polyclonal anti- $\beta$ -galactosidase (Europa Bioproducts, Cambridge, UK), anti-GFAP (glial fibrillary acidic protein) (Sigma-Aldrich, St. Louis, MO), and mouse monoclonal anti-CNPase (Covance, Berkeley). Sections were then incubated with the biotinylated anti-rabbit and anti-mouse IgG included in the ABC vector kits (Vector Laboratories, Burlingame, CA) that were used throughout the procedure according to the manufacturer's instructions.  $\beta$ -galactosidase staining was revealed with DAB (Black) and GFAP and CNPase stainings were revealed with streptavidin Cy<sup>TM</sup>3 complex (Vector laboratories).

## Primary Glial Cell Cultures

Glial cells were isolated from newborn Sprague-Dawley rat cortices essentially as described previously (McCarthy and de, 1980). Briefly, brain cortices were dissociated in HBSS (Invitrogen) containing 0.01% trypsin and 10  $\mu$ g/mL DNase I type IV (Sigma) for 10 min at 37°C. After centrifugation, cells were resuspended in DMEM containing 20% FCS, 4.5% glucose, 1% sodium pyruvate, 1% L-glutamine, and penicillin/streptomycin (Invitrogen), and filtered through a 70  $\mu$ m mesh. The cells were grown on poly-D-Lysine flasks (BD Biosciences, Franklin Lakes, NJ) until confluent (approximately 7–9 days). At confluency, the flasks were rotated at 150 rpm for 1 h at 37°C. The detached microglia were collected and used in further experiments. Cell medium was replaced and the flasks rotated for 18–20 h. The detached OL precursor cells (OPCs) were filtered and resuspended in DMEM containing GlutaMAX<sup>TM</sup> I and sodium pyruvate, 0.1% BSA (fraction V) (Invitrogen), 30 nM Na-selenite (Sigma), 10 nM D-biotin (Sigma), 10 nM hydrocortisone (Sigma), 50  $\mu$ g/mL insulin (Sigma), 50  $\mu$ g/mL apotransferrin (Sigma), 10 ng/mL PDGF-AA (Sigma), and 10 ng/mL bFGF (Abcys SA, Paris, France). To induce OPC differentiation, cells were grown for 3 days in the presence of 30 nM T3 (Sigma), 20 ng/mL recombinant human CNTF (R&D systems, Minneapolis, MN), and 10  $\mu$ M forskolin (Sigma). The remaining adherent astrocytes were detached using trypsin-EDTA (Invitrogen) and plated in DMEM containing 20% FCS.

## GLIALCAM EXPRESSION IN THE CNS

637

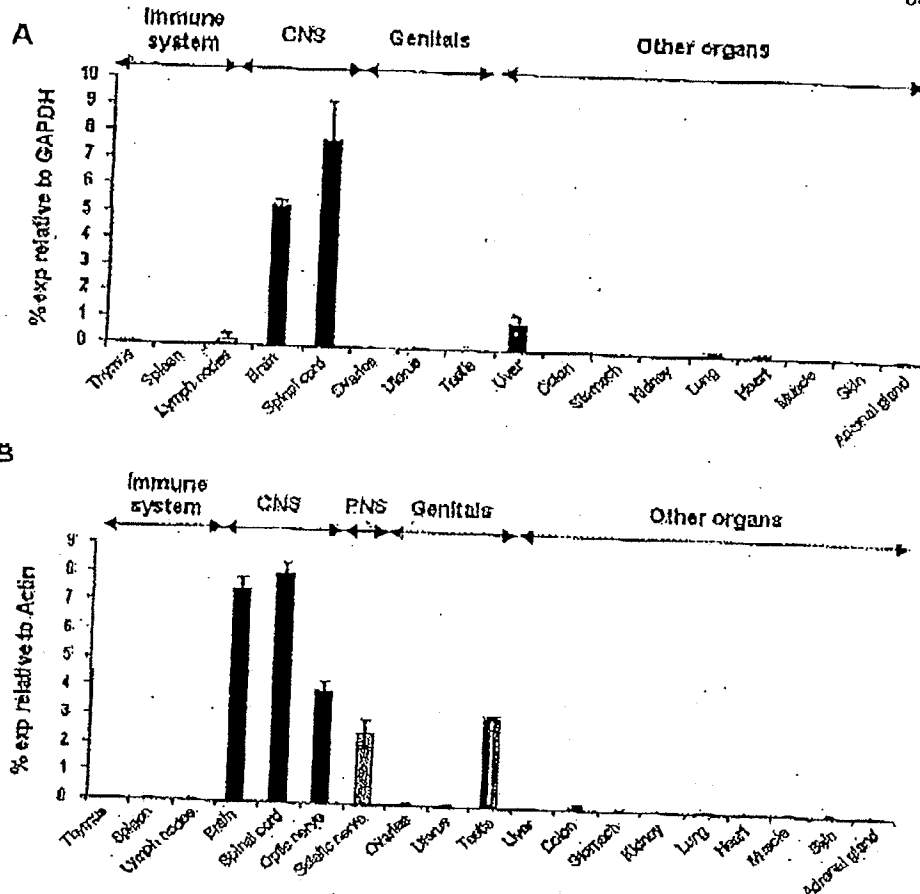


Fig. 2. *GlialCAM* gene expression profiling in human and mouse tissues. cDNA from human and mouse tissues were subjected to real-time quantitative PCR using specific primers for *GlialCAM*. *GlialCAM* expression was normalized to the internal housekeeping genes human *GAPDH* (A) and mouse *actin* (B). Human data are the mean of three experiments performed on the same cDNA set, while mouse data represents mean expression in three animals.

(1:200). Cells were then incubated for 1 h at room temperature with secondary antibodies: Cy<sup>TM</sup>3-conjugated donkey anti-rabbit and Cy<sup>TM</sup>2-conjugated donkey anti-mouse IgG (1:100 dilution; Jackson ImmunoResearch, West Grove, PA) after which the slides were mounted with Fluoromount (SouthernBiotech, Birmingham, AL) and visualized using a fluorescence microscope (Zeiss, Thornwood, NY).

tein. The homology between mouse and rat *GlialCAM* protein is 73% (Fig. 1B). The identity between human and mouse amino acid sequence is even stronger within the extracellular domain of the protein where there is 99% sequence conservation. Therefore, the extracellular domain was chosen to produce *GlialCAM* rodent and human specific antibodies.

## RESULTS

### *GlialCAM* Structure and Sequence

In Fig. 1A, we have illustrated the *GlialCAM* gene and protein domains. The gene contains 7 exons and encodes a 416 amino acid protein. The protein is composed of an extracellular region containing two Ig-like domains, one V-set and one C2 domain; a transmembrane region and a low complexity, proline-rich intracellular region (Moh et al., 2005). The structure of *GlialCAM* is similar to several members of the CTX (cortical thymocyte marker in *Xenopus*) gene family of adhesion molecules such as JAM and ESAM (Chung et al., 2005).

Homology searches of rat, mouse, and human amino acid sequences revealed that human *GlialCAM* is 94% identical to the mouse protein and 69% to the rat pro-

### *GlialCAM* is Strongly Expressed in the Nervous System

We first used real-time quantitative RT-PCR to analyze *GlialCAM* expression in a variety of adult human and mouse tissues. In human tissues, we observed that *GlialCAM* was highly expressed in the CNS and was only expressed at low levels in liver (Fig. 2A). Interestingly, in mouse tissues (Fig. 2B), *GlialCAM* was also observed in the CNS but not in the liver. In mouse, *GlialCAM* mRNA was present in the sciatic nerve. *GlialCAM* was also detected in mouse but not human testis. None of the other human and mouse tissues tested expressed *GlialCAM* mRNA. Overall, these data demonstrate that the predominant site of *GlialCAM* expression in human and mouse is in the NS rather than in liver, where the protein has previously been characterized.

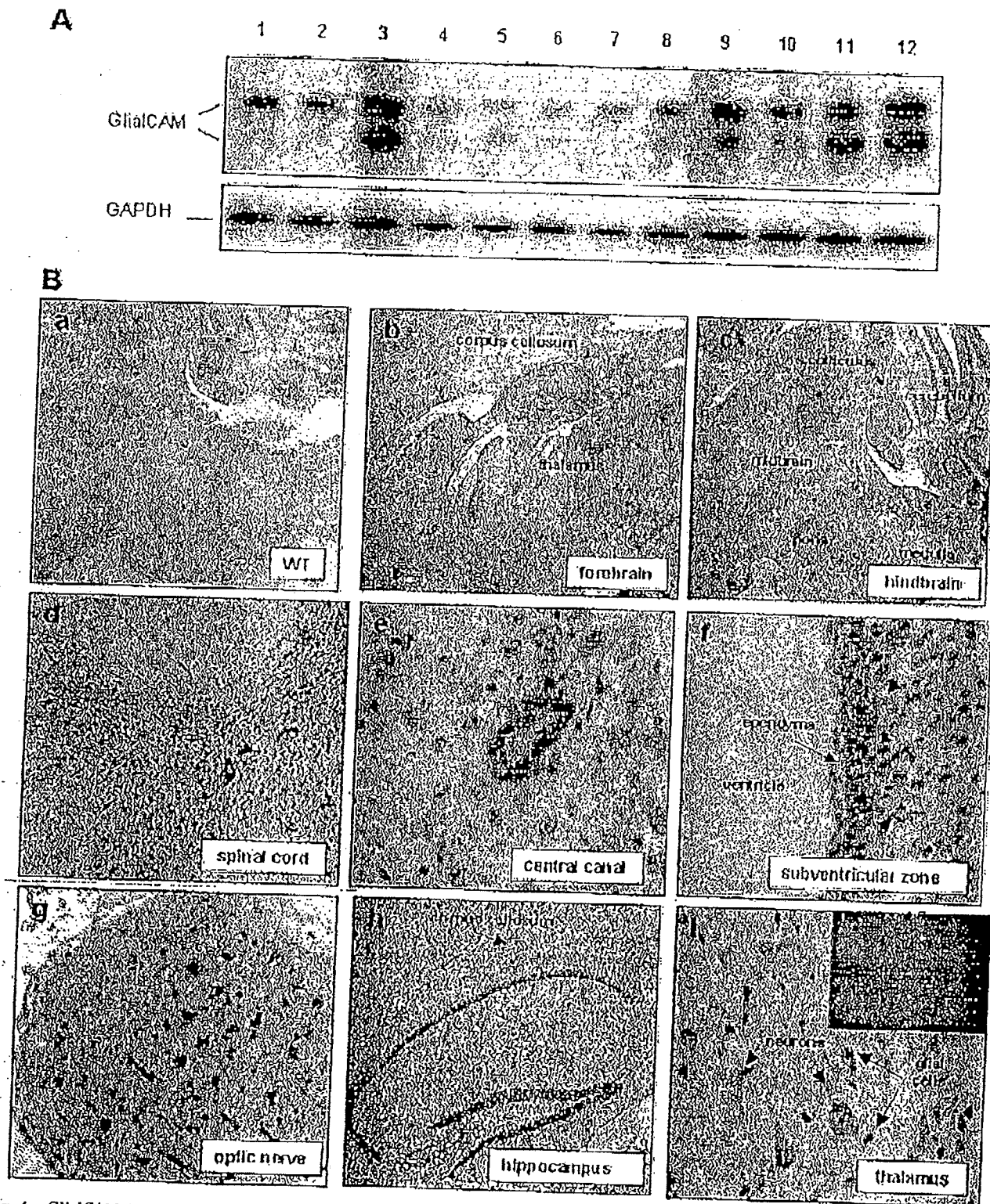


Fig. 4. GlialCAM distribution in mouse CNS. A: GlialCAM expression was tested by WB on various CNS regions of an adult *Flu/c* mouse. Strongest expression was detected in glia rich areas of brain and spinal cord. Lanes are as follows: 1, frontal cortex; 2, posterior cortex; 3, cerebellum; 4, hippocampus; 5, olfactory bulb; 6, striatum; 7, thalamus; 8, midbrain; 9, entorhinal cortex; 10, pons; 11, medulla; 12, spinal cord. B: *LacZ* reporter gene assay on GlialCAM heterozygous mouse brain, spinal cord, and optic nerve. Strong  $\beta$ -galactosidase activity was observed throughout the fore- (b) and hindbrain (c) but not in

control WT littermates (a). In the spinal cord (d) GlialCAM was expressed in the gray and white matter and in the ependymal cells of the central canal (e). In addition, in the lateral ventricles (f) the ependymal (arrow) and subependymal layers (arrowhead) are stained. Within the optic nerve (g), the corpus callosum (h), and the thalamus (i), staining is seen in glial cells. Finally, using double staining (j, insert)  $\beta$ -galactosidase activity (black, anti- $\beta$ -galactosidase antibody) was seen (black, anti- $\beta$ -galactosidase antibody) in CN1ase positive OL (red fluorescence).

## GLIALCAM EXPRESSION IN THE CNS

641

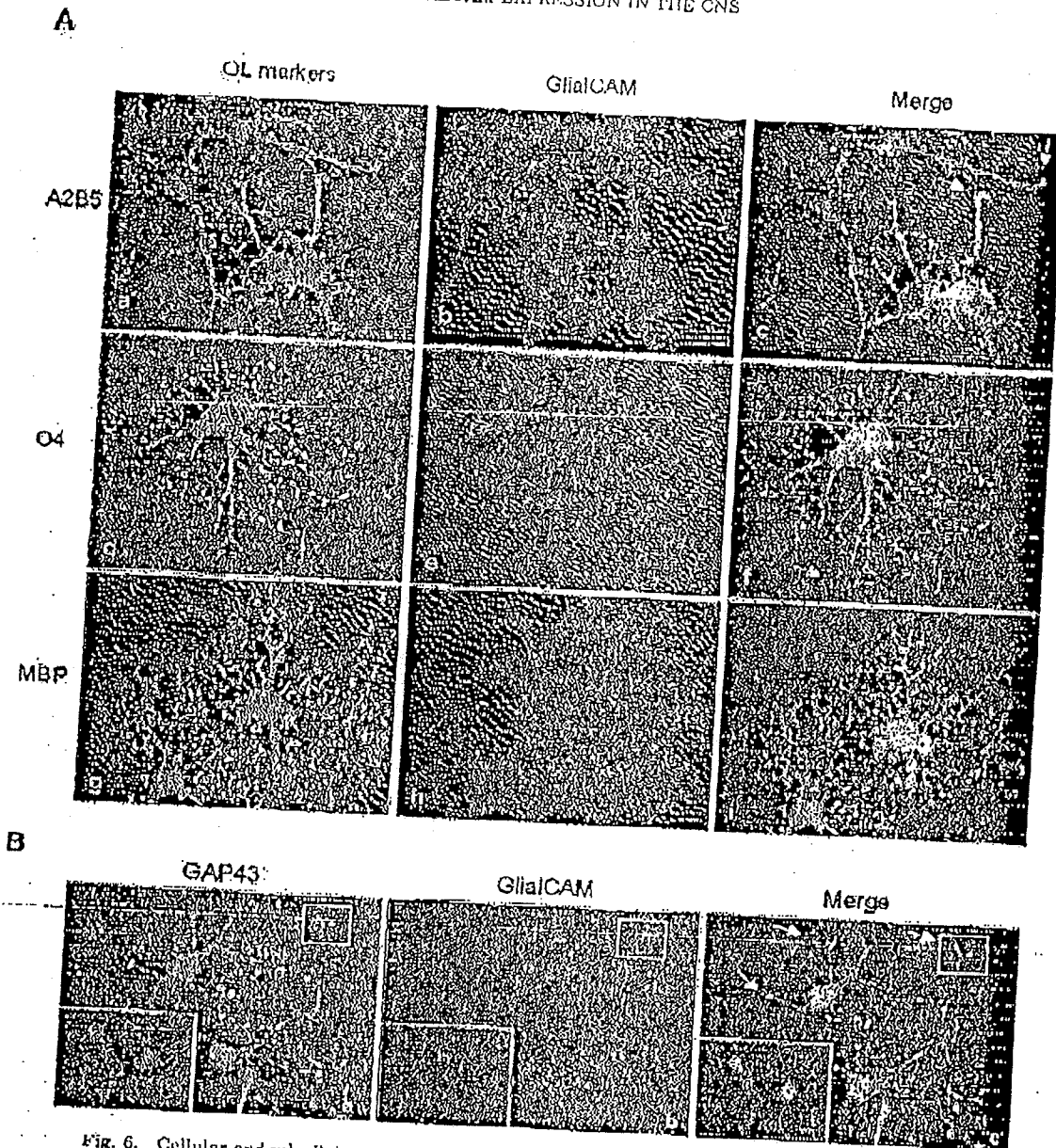


Fig. 6. Cellular and subcellular localization of GlialCAM in primary OL at different maturation stages. A: Immunocytochemistry using OL differentiation markers A2B5, O4, and MBP on purified OL shows that GlialCAM is detected in all three differentiation stages. Note that GlialCAM is expressed in the protruding tips (C) of early stage OLs. B: GlialCAM immunostaining colocalized with GAP43 (white arrows) in OPCs, indicating localization in growth cone-like structures. Higher magnification inset is seen in the left corner.

ous stages of postnatal development (P0–P21) and in adults. As shown in Fig. 5A, low amounts of mRNA were already detectable at birth (P0) and a steady increase of expression was seen from postnatal stage P10 to P21. Interestingly, the profile of GlialCAM expression follows that of MBP. GlialCAM protein expression was then studied by WB and the two specific bands were quantified individually by densitometry and normalized to GAPDH levels. As shown in Fig. 5B, the upper 63 kDa GlialCAM band is already detectable at

birth, increasing in intensity during postnatal development until P21 and decreasing slightly in adult animals. Starting from day 7 after birth, a second lower MW GlialCAM band ( $\approx 55$  kDa) appears which also increases in the later postnatal stages, but did not show a significant decrease in adult brain. In summary, our results demonstrate that GlialCAM mRNA and protein are upregulated during postnatal CNS development. Its coordinated expression with MBP suggests that GlialCAM might be expressed in various stages of the OL lineage.



mouse brain, or if it is upregulated in models of reactive gliosis.

## DISCUSSION

In the present study, we provide evidence that *GlialCAM*, previously identified as a putative tumor suppressor gene in human liver, is strongly and predominantly expressed in the human and mouse NS. In murine CNS, we demonstrate strong expression in various CNS regions like the cerebellum, the entorhinal cortex, the pons, the medulla, and the spinal cord. OL were identified as the major cell type expressing *GlialCAM* *in vivo*. In addition, we also observed strong expression of *GlialCAM* in ependymal cells along the brain ventricles and the central canal of the spinal cord. A potential role of *GlialCAM* in myelination was further supported by its temporal upregulation during postnatal mouse brain development, where it is coordinately expressed with MBP. *In vitro*, *GlialCAM* protein expression was detected in three developmental stages of the OL lineage. In A2B5 and O4 positive OL, *GlialCAM* colocalizes with GAP43 in OL growth cone-like processes. *GlialCAM* was also observed in primary astrocytes. Taken together, the present data indicate a potential function for *GlialCAM* in OL, astrocyte, and ependymal cell biology.

The *GlialCAM* sequence shares similarities with members of the CTX (cortical thymocyte marker in *Xenopus*) family of adhesion molecules including JAM-3 and ESAM (Chung et al., 2005). These members have been identified as trans-membrane components of tight junctions (TJ) in a wide range of tissues in endothelial and/or epithelial cells (Arrate et al., 2001; Eguchi et al., 2005; Hirata et al., 2001). Although the precise physiological role of *GlialCAM* remains to be elucidated, its significant homology to the CTX family together with its overall expression pattern might indicate a potential function in the formation of TJ like structures in OL, astrocytes and in the CNS ependyma.

The CNS ependyma is made of a single layer of ciliated epithelial cells named ependymal cells, which function as a protective and metabolic barrier between the CNS and CSF (Del Bigio, 1995). Ependymal cells are interconnected via numerous gap junctions, and some ependyma also express TJ associated proteins such as occludins and ZO-1 (Lippoldt et al., 2000; Petrov et al., 1994). Future studies using *GlialCAM* deficient mice might help to elucidate the potential role of *GlialCAM* in the CSF/CNS barrier. In addition to the ependymal cell expression, *GlialCAM* positive cells were detected in the sub-ependymal layer of the lateral ventricles. The sub-ventricular zone, the adult derivative of the embryonic forebrain germinal zones, is a site of neurogenesis and gliogenesis in the adult mammalian brain (Menn et al., 2006; Varoz-Buylla and Garcia-Verdugo, 2002). Further studies are needed to unravel a potential function of *GlialCAM* in these cellular functions.

Astrocytes do not form regular TJ in normal conditions but were shown to express the TJ associated pro-

tein claudin-1 under proinflammatory conditions, suggesting the formation of rudimentary TJs at astrocyte/astrocyte contacts during reactive astrogliosis (Duffy et al., 2000). We were unable to detect clear *GlialCAM* expression on astrocytes *in vivo* by *LacZ* staining, although the pattern of expression suggested that some of the positive cells might be astrocytes. In contrast, *in vitro* immunocytochemistry studies clearly showed strong *GlialCAM* expression in primary rat astrocytes expressing the reactive astrocyte marker, GFAP. The strong expression *in vitro* might be explained by the fact that cultured astrocytes are in a different activation state than resting astrocytes *in vivo*. Further studies are needed to investigate the role of *GlialCAM* in astrocytes, like its behavior on proinflammatory challenge *in vitro* or during reactive astrogliosis *in vivo*. In a confluent astrocyte layer, the protein is particularly localized at cell-cell contact sites. This observation is in accordance with a recent study showing that in a confluent culture of stably transfected MCF7 cells (human breast carcinoma cells), *GlialCAM* was recruited to the sites of cell-cell attachment (Moh et al., 2005). However, in low-density astrocyte cultures, we observe that the protein is localized at the tip of cell processes. This expression is in line with the observation by Moh et al., that at a lower cell density, *GlialCAM* is localized to punctuate structures in the perinuclear membrane, cytoplasm, and at the tip of the cell surface protrusions of stably transfected MCF7 cells (Moh et al., 2005). The expression of *GlialCAM* in the processes of bipolar astrocytes also suggests a role for this molecule in process extension or differentiation. Together, these observations suggest a function for *GlialCAM* in astrocyte/astrocyte and astrocyte/extracellular matrix interactions as well as in astrocyte growth and migration.

Unlike astrocytes, OL express TJ like structures under normal conditions. OSP/claudin-11, a major component of CNS myelin, is known to form TJ strands within myelin sheaths and has been proposed to have a structural role in myelin formation and maintenance (Gow et al., 1999; Morita et al., 1999). Based on our observation of *GlialCAM* expression in white matter regions of the adult brain and in primary, MBP-positive mature OL *in vitro*, *GlialCAM* might play a similar role in maintaining the myelin structure. In addition, the postnatal expression profile of *GlialCAM*, which correlates with MBP levels and myelin formation, supports a role for *GlialCAM* in myelination and/or in the maintenance of the myelin sheaths.

We have also shown that in cultured OL, *GlialCAM* is expressed in early differentiation stages and colocalizes with GAP-43 to the tips of the processes. GAP-43 is a regulator of cytoskeletal organization known to mediate neuronal growth cone navigation (Meiri et al., 1986). Growth cones are found at the tip of growing axons and have the ability to respond to extracellular directional cues and to mediate target recognition (Strittmatter et al., 1995). Little is known about growth cones in OL, but recent data suggest the existence of such structures

## GLIALCAM EXPRESSION IN THE CNS

645

- Ramsby M, Afsari F, Stark M, Huglison E. 2003. Microfilament and microtubule organization and dynamics in process extension by central glia-4 oligodendrocytes: Evidence for a microtubule organizing center. *Glia* 42:118-129.
- Sakisaka T, Takai Y. 2005. Cell adhesion molecules in the CNS. *J Cell Sci* 118:5407-5410.
- Sherman DL, Brophy PJ. 2005. Mechanisms of axon ensheathment and myelin growth. *Nat Rev Neurosci* 6:688-690.
- Spiegel I, Adamsky K, Eisenbach M, Eshed Y, Spiegel A, Mirsky R, Scherer SS, Peles E. 2006. Identification of novel cell-adhesion molecules in peripheral nerves using a signal-sequence trap. *Neuron Glia Biol* 2:27-38.
- Strittmatter SM, Pankhausser C, Huang PL, Machimo H, Fishman MC. 1995. Neuronal pathfinding is abnormal in mice lacking the neuronal growth cone protein GAP-43. *Cell* 80:445-452.
- Valenzuela DM, Murphy AJ, Frendaway D, Gale NW, Economides AN, Auerbach W, Poueymirou WT, Adams NC, Rojas J, Yarechak J, Chernomorsky K, Baucher M, Elsasser AL, Esau L, Zheng J, Griffiths JA, Wang X, Su H, Xue Y, Dominguez MG, Noguera I, Torres R, Macdonald LE, Stewart AF, DeChiara TM, Yancopoulos GD. 2003. High-throughput engineering of the mouse genome coupled with high-resolution expression analysis. *Nat Biotechnol* 21:652-659.
- Alvarez-Buylla A, Garcia-Verdugo JM. 2002. Neurogenesis in adult sub-ventricular zone. *J Neurosci* 22:629-634.



# EXHIBIT 1

SeqA Name	Len(aa)	SeqB Name	Len(aa)	Score
1 SEQ20-EC	240	2 SEQ22-Ecmat	207	100
1 SEQ20-EC	240	3 AAE14784-IGFSP4	298	100
2 SEQ22-Ecmat	207	3 AAE14784-IGFSP4	298	100

CLUSTAL 2.0.10 multiple sequence alignment

```

SEQ20-EC      MKRREGALSRRASRALRLAPFVYLLLIQTDPLEGVNITSPVRLIHGTVGKSALLSVQYSST 60
AAE14784-IGFSP4 MKRREGALSRRASRALRLAPFVYLLLIQTDPLEGVNITSPVRLIHGTVGKSALLSVQYSST 60
SEQ22-Ecmat    -----VNITSPVRLIHGTVGKSALLSVQYSST 27
                *****

SEQ20-EC      SSDRPVVKWQLKRDKPVTVVQSIGTEVIGTLRPDYRDRIRLFENGSLLLSDLQLADEGTY 120
AAE14784-IGFSP4 SSDRPVVKWQLKRDKPVTVVQSIGTEVIGTLRPDYRDRIRLFENGSLLLSDLQLADEGTY 120
SEQ22-Ecmat    SSDRPVVKWQLKRDKPVTVVQSIGTEVIGTLRPDYRDRIRLFENGSLLLSDLQLADEGTY 87
                *****

SEQ20-EC      EVEISITDDTFTGEKTINLTVDVPISRPQVLVASTTVLELSEAFTLNCSHENGTKPSYTW 180
AAE14784-IGFSP4 EVEISITDDTFTGEKTINLTVDVPISRPQVLVASTTVLELSEAFTLNCSHENGTKPSYTW 180
SEQ22-Ecmat    EVEISITDDTFTGEKTINLTVDVPISRPQVLVASTTVLELSEAFTLNCSHENGTKPSYTW 147
                *****

SEQ20-EC      LKDGKPLLND SRMLLSPDQKVLTI TRVLMEDDDLYSCMVENPISQGRSLPVKITVYRRSS 240
AAE14784-IGFSP4 LKDGKPLLND SRMLLSPDQKVLTI TRVLMEDDDLYSCMVENPISQGRSLPVKITVYRRSS 240
SEQ22-Ecmat    LKDGKPLLND SRMLLSPDQKVLTI TRVLMEDDDLYSCMVENPISQGRSLPVKITVYRRSS 207
                *****

SEQ20-EC      -----
AAE14784-IGFSP4 LYIILSTGGIFLLVTLVTVACACWKPSKRKQKKLEKQNSLEYMDQNDRLKPAPKDHSP 298
SEQ22-Ecmat    -----

```